POLARIZED LIGHT FROM STAR FORMING REGIONS

DAVID A. WEINTRAUB
Vanderbilt University

ALYSSA A. GOODMAN
Harvard University

and

RACHEL L. AKESON
University of California, Berkeley

Studies of polarized radiation from molecular clouds and the environments of **protostars** are providing information about the orientations and strengths of magnetic fields and the sizes and compositions of dust grains in these environments. This relationship between **dust grains**, **magnetic fields**, and polarized light exists because dust grains aligned by magnetic fields will polarize background starlight which otherwise would be unpolarized and will emit intrinsically polarized thermal radiation; also, even unaligned dust grains will scatter photons and so the dusty environments of young stars often produce reflection nebulae. Importantly, some of the observational results are providing the first ever measurements of magnetic field alignments and strengths on scales from 1000 AU to 10s of parsecs in dense cores and molecular clouds; such measurements are particularly valuable for understanding the mechanisms of star formation and the importance of magnetic fields and outflows. In addition, polarization studies are driving ideas that the size distributions and compositions of populations of dust grains around **YSOs** may be quite different from those assumed for astrophysical dust in the **ISM**. This astrophysically important information is unavailable, at present, from any other types of measurements.

young stellar objects

I. INTRODUCTION

Polarization studies have progressed enormously since the era of PPIII, including a huge expansion in the field of measuring polarized thermal emission from dust grains at far-infrared through millimeter wavelengths. Both linear and circular polarization observations and the modeling of those observations in terms of the relative contributions

of scattering and dichroic extinction and emission are contributing to our understanding of the relationship between magnetic fields, circumstellar disks and young stellar outflows and of the properties of dust grains, from the interstellar medium (ISM) to dark clouds to protostellar nebulae; in addition, thermal emission polarimetry now informs us about the large and small scale magnetic field structure in star forming regions. In the 1990s, we have witnessed enormous improvements in computational modeling and the development of multiple techniques for obtaining polarimetric data on many telescopes and at many wavelengths. Thus, with many more theorists, telescopes and observers involved in polarimetry studies, this field of research has become an area of significant astrophysical import.

In the first part of this chapter, we discuss how observations of polarized background starlight, at both optical and near-infrared wavelengths, and polarized thermal emission from dust at far-infrared and millimeter wavelengths, can be used to chart out magnetic fields in star-forming regions. In the second part, we describe how nebulae around YSOs can be studied by measuring the polarized, scattered light that emerges from these dusty environments at optical and near-infrared wavelengths.

II. MAPPING MAGNETIC FIELDS

Magnetic fields introduce asymmetries into physical systems that often can be detected via polarimetric observations. In the ISM, and in circumstellar environments, magnetic fields impose these asymmetries by attempting to align dust particles with the direction of local field lines. As the reader will see below, magnetic fields are more successful in coaxing dust grains into line in some regions than they are in others. With any degree of success though, the grains become partially aligned along some preferred (magnetic field) direction. Consequently, background starlight passing near them will become partially polarized and light emitted by these dust grains will be partially polarized.

From the standpoint of polarimetry as it is done in 1998, there are two kinds of star-forming regions. "Dark cloud complexes" harbor embedded protostars found alone or in small groups. The densest parts of these regions are apparent as "dark" clouds ($0.5 < A_V < 10$ mag) on optical photographs and as moderate-level ($\sim 10 - 100$ MJy Sr^{-1} at 100 μm) extended emission in the IRAS survey. To date, po-

larimetry of background starlight has been the principal tool used in mapping magnetic fields in dark clouds. "Massive star-forming regions" are regions where most embedded protostars are found in large clusters (>> 10 stars forming together). Optically, these regions often show up as high extinction black patches interspersed with bright reflection and/or emission nebulae. The peak amounts of thermal dust emission from these regions (typically $> 10^4$ MJy Sr^{-1} at 100 μm) far exceed those in dark clouds. At present, magnetic fields in massive star-forming regions can be mapped with thermal emission polarimetry at parsec and sub-parsec scales. However, in all but the brightest, warmest peaks of dark clouds, thermal emission polarimetry is still not feasible. This situation should change over the next few years, when satellite-based far-infrared polarimetry becomes a reality, and as ground-based millimeter and submillimeter instruments become more sensitive.

A. Dark cloud complexes

In order to understand what polarization maps can tell us about dark clouds, it is necessary to fully understand how and why the dust in dark clouds polarizes background starlight. If every dust grain along the line of sight to a background star were the same size, shape, and composition, and aligned to the same degree, by a magnetic field whose direction with respect to the line of sight never changed, polarization maps would be easy to interpret. In that case, the ensemble of photons passing through a sea of similar grains would become systematically more highly polarized after each encounter. Because grains tend to align with their shortest axis parallel to the field (see Figure 1; see also http://cfa-www.harvard.edu/ agoodman/ppiv/ which contains additional figures not shown in this printed review), the polarization direction observed would give the direction of the magnetic field as projected onto the plane of the sky. In this simple case, the percentage of polarization observed (p) would rise linearly with the number of grains, which in turn is proportional to the extinction, A_V.

Figure 1

Reality, however, is not so simple. Not all grains are similar, they are not all equally willing to align, and field lines are not straight, and non-magnetic field mechanisms can also align grains. Therefore, we need models of the grain distribution, the alignment distribution, and the field structure, before we can learn about magnetic fields from polarization maps.

Dark clouds and star-forming regions represent a special challenge in the interpretation of background-starlight polarization maps, because grains in those regions seem to have properties unlike those in the general ISM (see Whittet 1992 and references therein). In the larger-scale ISM, the interpretation of polarization maps (see, e.g., the Mathewson and Ford 1970 map of the local Galactic region), is easier, because grain properties "average out" over long lines of sight (see Heiles 1996).

Figure 2 shows an optical polarization map of Taurus, superimposed on the IRAS Sky Survey Atlas (ISSA) 100 μm map. The most striking feature of the Taurus polarization map is the smoothness of the overall pattern. There are no obvious topological changes in the field caused by the presence of the dark clouds (Goodman et al. 1990). Recent MHD modeling shows that this lack of structural change can be expected in the case where the field and kinetic energies are roughly equal (Ostriker, Gammie, and Stone 1998, submitted). Nonetheless, one cannot help wondering whether the field *inside* dark clouds might be in a different direction, or have a different dispersion, than that in cloud environments. Since background starlight polarimetry cannot be used where background stars are not visible, optical observations are useful only up to about $A_V \sim 2$ mag. Near-infrared polarimetry of background stars, though, can see in to as much as $A_V \sim 40$ mag (see, e.g., Wilking et al. 1979).

Figure 2

In cold dark clouds, near-infrared polarization maps look *exactly the same* as expected by extrapolating from optical polarimetry obtained around the clouds peripheries. Figure 3 shows a comparison of optical and near-IR polarization position angles for the dark cloud B216-217 (region highlighted by the horizontal rectangle in Figure 2). The near-IR map, which covers interior portions of the cloud too opaque for optical polarimetry, looks simply like a shrunken version of the optical map (see Goodman et al. 1992). Fits to the polarization position angle distributions are identical within the errors (Figure 3). So, either the field in the dense part of B216-217 is topologically exactly the same as in the lower-density cloud environment, or the polarization observations are somehow insensitive to the dust in the dark cloud.

Figure 3

Polarization-extinction relations show, definitively, that polarimetry measurements of background starlight are insensitive to magnetic fields in dark clouds (Goodman et al. 1995; Gerakines et al. 1995; Arce

et al. 1998). As is shown in Figure 4, polarization percentage does not rise with extinction in cold dark clouds. This means that while cold dark clouds contribute a great deal of extinction, they contribute no polarization; so, polarization maps are insensitive to the field there. Why? It is likely that grain alignment mechanisms are far more efficient in the warmer, lower-density ISM than they are in dark clouds (see Lazarian et al. 1997). Thus, the polarization along a line of sight through a dark cloud is strongly dominated by dust interactions *not* taking place in the dense interiors of dark clouds. It is as if the dark cloud is invisible from the standpoint of polarizing background starlight (see Goodman et al. 1995).

Figure 4

The polarization-extinction plots in Figure 5 represent an attempt to quantify the conditions where interstellar material goes from being "good" at polarizing background starlight to being "bad." In the "good" regions, it is safe to use background-starlight polarimetry to map fields, and in the "bad" regions, it is not. The plots show that a polarization-extinction relation constructed for the "cut" through Taurus shown in Figure 2 exhibits two clear trends. The stars background to the "general low-density ISM" show a linear rise in polarization with extinction, while those behind the cold dark clouds show a flat $p - A_V$ relation like those shown using near-IR data in Figure 4. These two trends cross at $A_V = 1.3 \pm 0.2$ mag, and Arce et al. (1998) identify this point as the "breakpoint" between good and bad regimes. This result implies that almost all stars form in regions of the ISM where background starlight polarimetry cannot effectively map the magnetic field, and other techniques need to be explored.

Figure 5

The "other technique" best suited for studying both dark clouds and warmer dense gas is thermal emission polarimetry. As mentioned above, this technique is currently most feasible in the warmer regions (which produce more thermal emission). The astute reader may have noticed that the lower panel of Figure 4 does show a small rise in polarization with extinction for the warmer clouds, and may wonder if that means that background starlight polarimetery is alright to use there. Unfortunately, the answer is still no. In those regions, there is tremendous confusion of the field in the region of interest, which typically lies at > 1 kpc distance with fields all along the line of sight to that region. An example of this problem can be seen by comparing the optical polarization map of M17 in Schulz et al. 1981, which shows

a messy, bimodal distribution of polarization vectors, with the far-infrared polarization map from the KAO (Dotson 1996) and the 800 μm polarization map from the JCMT (Vallée and Bastien 1996) which show very smooth distributions of vectors for the same region (see Figure 4 of Goodman 1995).

B. Magnetic fields on large scales in molecular clouds

As observations of selective absorption rely on sufficient flux from background sources, these measurements become difficult in dense regions with high extinction. However, the same aligned dust grains that produce selective extinction in the optical and near-infrared emit polarized radiation in the far-infrared to millimeter regimes (Figure 1). The cross sections for absorption and scattering at far-infrared and longer wavelengths are very small, ensuring in almost all cases that the polarization is due to emission from aligned grains. The significant column densities necessary to detect far-infrared to millimeter wavelength polarized emission generally restricts these observations to warm molecular clouds and areas of active star formation. For example, a column density $> 5 \times 10^{22}$ cm^{-2} ($A_V \sim 25$) is necessary with current instrumentation for detection of polarized emission at 350 μm (Schleuning, personal correspondence). Thus, one advantage of these measurements is that the polarized emission is not affected by low column density material. In this section, we will discuss observations of polarized thermal emission from dust made over large regions of molecular clouds and discuss the Orion molecular cloud in detail.

Observations in the far-infrared are sensitive mainly to warm (T $\sim$ 50 K) dust, while (sub)millimeter observations probe the entire dust column. Given the resolution currently available at far-infrared and submillimeter wavelengths, these observations trace the field structure on scales from 0.05 pc in Orion to 1 pc in SgrB2.

One of the most remarkable results of far-infrared polarimetry is that polarized emission is detected from the vast majority of locations observed (Hildebrand 1996). This implies that aligned grains are the rule rather than the exception in warm molecular clouds. Based on over 500 independent measurements, Hildebrand (1996) found that the maximum polarization observed is 9%, while the median value of p is near 2%. The observed magnetic field direction is generally orderly over the entire map region (Figure 6), which covers from 0.3 pc in DR21 to 5 pc in SgrB2 (see, e.g., M17: Dotson 1996 and Vallée and Bastien

1996); SgrB2: Dowell 1997, Novak et al. 1997; DR 21: Minchin and Murray, 1994, Glenn et al. 1998; W3: Greaves et al. in prep.).

Figure 6

Another attribute of the far-infrared and (sub)millimeter observations with several pointings within a cloud is that the polarization percentage (p) decreases toward the regions of highest optical depth. Several pieces of information are known about this so-called "polarization hole" effect. 1) The decrease in p is more than expected from opacity effects. 2) Unlike for optical observations, the polarized flux increases in the regions of highest total flux up to extinctions of at least $A_V = 300$ (Schleuning et al. 1996), although p decreases. 3) The polarization percentage is not correlated with dust temperature (Dotson 1996). Various proposed explanations for polarization holes include: small scale (compared to the resolution) field structure, decreased grain alignment with higher density or spherical grain growth.

As a specific example of polarized emission observations of a massive star-forming region, we discuss measurements of the Orion molecular cloud (OMC), including the observed polarization hole. Many groups have observed selected objects or limited regions within OMC, but the large scale (1 parsec) field structure was only recently mapped by Schleuning (1998). The magnetic field structure is extremely orderly on this scale although there are symmetric deviations of 25° from the average field direction (Figure 7). Schleuning interprets this curvature as field pinching with a radius of 0.5 pc. The Kleinmann Low (KL) nebula, which includes the energetic object IRc2, has been observed by many groups in polarized emission at wavelengths from 100 μm to 3 mm. Single-dish observations over several positions near KL invariably find that p decreases toward IRc2 (Gonatas et al. 1990. Leach et al. 1991. Schleuning et al. 1996. Aitken et al. 1997). Recent interferometric observations at millimeter wavelengths by Rao et al. (1998) at higher resolution reveal significant structure in the polarized emission near IRc2 (Figure 7). Thus, the polarization hole at Orion KL appears to be due to averaging of varying polarization directions within the single-dish beams; however, more high resolution observations are necessary to determine if the decrease in p is always due to unresolved field structure.

Figure 7

C. Observations of Individual Embedded Protostellar Objects

Observing the magnetic field structure toward individual YSOs requires high resolution and sensitivity to relatively cool (<50 K) dust.

Current telescope sensitivity levels limit detections of polarized emission to regions with high dust columns ($> 10^{24}$ cm^{-2} at 1 mm). Although only a handful of YSOs have been observed in polarized emission to date, the number is increasing as telescope sensitivities increase. Sources with a range of stellar mass have been observed, although the observations tend to concentrate on younger, embedded sources, such as the Class 0 YSOs. These observations are the best method to directly measure the field structure in protostellar envelopes and disks.

One aspect of star formation involving magnetic field structure is the modeling of bipolar outflows which, it is generally assumed, require the presence of magnetic fields. Comparison of the measured magnetic field and outflow directions may provide important constraints on the theories. In some sources, such as NGC 1333 IRAS 4A (see, e.g., Akeson and Carlstrom 1997) and NGC 7538 IRS 11 (Minchin and Murray 1994), the field direction and the outflow appear to be very well aligned. However, toward other sources, such as VLA 1623, which drives a well collimated molecular outflow, the magnetic field direction and the outflow are nearly orthogonal (Holland et al. 1996). Some authors (Greaves et al. 1997, Minchin et al. 1996) suggest that the observed angle between the magnetic field and the outflow may be a function of the viewing angle. We caution, however, that outflow inclination angles often are poorly determined and that some of the sources are binaries with multiple outflows while the polarization has been measured only for the entire system. We also note that polarization observations measure the field direction in the plane of the sky and any observed correlations on the sky do not guarantee correlation in three dimensions.

Most observations of magnetic fields toward YSOs are unable to resolve structure within the protostellar disk and envelope. A typical single-dish resolution of 10"-15" yields a beam of 1500–2000 AU in Taurus, yet low mass protostellar disks are generally $\leq$ 100 AU (see chapter by Wilner and Lay) and envelopes are 1000s of AU. These observations generally include emission from the protostellar envelope, disk and even contributions from the surrounding core for measurements at higher frequencies. Thus while fields can be characterized as poloidal or toroidal depending on the relative angles of the outflows and/or disks, the measured fields are weighted averages over all field components present in a beam. High resolution, interferometric obser-

vations have been made for NGC 1333 IRAS 4A (Figure 8). These 3 mm observations are sensitive only to emission from the densest parts of the protostellar disk and envelope, with a lower limit to the H_2 density of 10^8 cm^{-3} in the observed material. These observations, in which structure was observed in the polarized emission on scales of 1000 AU, are evidence against a decrease in grain alignment at higher densities. Akeson and Carlstrom modeled the data using an hourglass field morphology within the envelope, where the field was aligned parallel to the outflow. Evidence for an hourglass field on a much larger (0.1 parsec) scale has been seen for the high mass source W3 IRS5 (Greaves et al. 1994) (Figure 6).

Figure 8

While (sub)millimeter polarimetry of individual sources has begun to reveal the role of the magnetic field, high resolution observations using interferometers and observations of many more sources, perhaps utilizing the new submillimeter bolometer arrays, such as SCUBA on the JCMT, are needed to constrain the role of the magnetic field.

III. MAPPING CIRCUMSTELLAR NEBULAE

Reflection nebulae, which are intrinsically polarized because we are observing scattered photons, are commonly found to surround YSOs when these objects are observed at optical and near-infrared wavelengths (see Figure 1). In this section, we concentrate on observations of the spatially resolved reflection nebulae, not on polarimetric observations of the central stars of these nebulae. Polarization observations of the stars themselves, taken through diaphragms centered on the stars, will invariably also include some light from the circumstellar nebula. In fact, aperture polarimetric observations that show unusually high polarization values provide a strong rationale for seeking polarimetric maps of such objects (although it also true that objects with low polarization values in aperture measurements may show significant polarization in maps). Aperture polarimetry work has been extensively reviewed in recent years by Grinin (1994; for Herbig Ae/Be stars), Bastien (1988; for T Tauri stars) and Bastien (1996; for YSOs). In addition, a compilation of all published polarimetric maps prior to 1990 is given by Bastien & Ménard (1990).

In general, reflection nebulae can be observed at a given wavelength if enough dust grains are present in the circumstellar environment, if the dust grains are large enough in comparison to the wavelength, and

if the YSO is an abundant source of photons at the selected wavelength. Under these conditions, some fraction of the light emerging from the protostellar photosphere scatters one or more times in the dust zone before emerging into interstellar space as polarized light. From these simple considerations, it is clear that the polarization signature of a reflection nebula, or the lack thereof, provides information about the density and size distribution of circumstellar dust and about the position of the central light source.

A. Scattering Models

For most of the 1990s, the working model for interpreting polarization maps obtained by observers has been that developed by Whitney and Hartmann (1992, 1993). In these and similar models, a Monte Carlo code is used to calculate polarization maps in dusty, circumstellar environments, using Mie scattering theory and assuming spherical dust particles. The work of Whitney and Hartmann built on the original work of Ménard (1989), who was the first to compute such Monte Carlo models, and the recognition by Bastien and Ménard (1988) that multiple scattering is essential in interpreting polarization maps. Additional work has been done by Fischer, Henning & Yorke, (1994, 1996) and Lucas and Roche (1997, 1998). The most important achievement of these models is in developing maps that produce qualitatively good matches to observed polarization maps of reflection nebulae around YSOs (Figure 9).

Figure 9

The ability of a population of dust grains to scatter (and thereby polarize) starlight depends on the sizes, shapes and compositions of dust grains present in an environment. The maximum degree of linear polarization (p_{max}) as well as the total amount of scattered light at a given wavelength depends strongly on the size of the dust grains relative to the wavelength of the incident photons. If the size parameter x is small, where $x = \frac{2\pi a}{\lambda}$ and a is the radius of a spherical dust grain, the particles are small compared to the wavelength and thus are in the Rayleigh scattering regime, wherein the scattering efficiency decreases as λ^4. This is unlikely to be the situation for dust grains and scattering in the optical or infrared.

In many cases, YSOs appear as bright reflection nebulae in the optical but as point sources in the near-infrared. In these cases, the dust grains are extremely effective at scattering 0.5 μm photons but equally ineffective at scattering photons at λ = 1-2 μm. For such nebulae,

dust distributions designed to match the ISM, such as MRN (Mathis et al. 1979) or that of Fischer et al. (1994), which have maximum grain sizes $a \leq 0.25$ μm and steep power laws describing the number of dust grains of a given size, e.g., $N(a) \propto a^{-3.5}$, and thus have almost no large dust grains, clearly are not appropriate. In these cases, strong evidence exists for a population of larger dust grains with different albedo and polarization properties. Alternative "large grain" models that have been proposed include that of Pendleton et al. (1990), with a maximum grain size of 0.8 μm, and the KMH grains of Kim et al. (1994), with a maximum grain size of 10 μm.

Most dust models include dust grains that are fairly reflective in the optical but become increasingly dark in the near-infrared. These models also appear to contradict what is observed. For example, Whitney et al. (1997) estimate a dust albedo $w \simeq 0.3 - 0.4$ at 2.2 μm from their polarization models, whereas the MRN distribution is barely half this value at the same wavelength. Similarly, Leinert et al. (1991) report a value of $w \geq 0.32$. Lucas and Roche (1998) argue that icy mantles on dust grains, which are common in molecular clouds and around YSOs, would tend to increase the dust albedos above that predicted for bare grains.

Thus, the next generation of models will need to include scattering properties of large grains (Figure 10 and 11). These will serve as an excellent complement to small grain models and will thereby allow observers to better determine the size and material properties of circumstellar dust grains around YSOs.

Figure 10
Figure 11

B. Identifying YSOs, Disk Orientations and Outflow Sources

One important way in which the models have contributed thus far is in showing that polarization "disks" mark the optically thick regions (i.e., the equatorial disk planes) of reflection nebulae (Figure 9). These polarization disks are regions close to the central stars where the polarization patterns clearly depart from centrosymmetry. Usually, the vectors in these regions are characterized by low ($\sim$ 10%) amplitudes and are roughly perpendicular to the symmetry axis of the bipolar nebula.

Bastien and Ménard (1988, 1990) demonstrated that polarization disks can be explained as the result of multiple scattering. In environments where stars have optically thick, but spatially thin disks, photons

that originate at the stellar photospheres cannot propagate radially outward within the disk plane; instead, they travel through the optically thin polar regions (in many cases evacuated by outflows) and scatter into the disk from above and below. Photons that scatter into the disk at sufficiently large radial distances from the star (where the disk itself has become optically thin) can scatter out of the nebula into our line of sight. This scenario produces maps with regions of low polarization that define the disk plane. In addition, the maps show centrosymmetry in which the original sources of photons, i.e. the protostars, lie at the origins (the polarization centroids) of the centrosymmetric maps. Thus, maps such as these are well suited for determining whether an intensity source is a (proto)star or a reflection nebula and whether an intensity source is actually the source of scattered photons in the nebula.

If circumstellar disks are the fairly small (radii $\leq$ 100 AU) accretion disks expected in protostellar collapse (e.g., Terebey, Shu and Cassen 1984) and spectral energy distribution models (e.g., Adams, Lada and Shu 1987), then in most cases, the observed light from polarization disks probably does not represent scattering from these disks themselves. Rather, because of the limited spatial resolution of most observations, a single pixel in an observational map almost certainly includes photons that scatter from material immediately above and below such disks (Whitney et al. 1997; Lucas and Roche 1998). However, it is possible that circumstellar disks are much larger, with radii of 10^3 - 10^4 AU, comparable to the pseudodisks modeled by Galli and Shu (1993) and to observations obtained by many workers in the submillimeter and millimeter regimes (see Weintraub et al. 1999). Many of the published polarization maps could, in fact, be resolving these large disks. In addition to identifying the presence and projected orientation of circumstellar disks, polarization maps also have been used to determine the inclination angles of the disks, through comparisons of the bipolar reflection nebulae with the Monte Carlo disk models.

The technique of using the polarization centroid to locate an embedded protostar has been applied successfully to polarization studies of the dark cloud L1287 (Weintraub and Kastner 1993), who discovered a bipolar reflection nebula centered on the position of IRAS 00338+6312. Notably, the IRAS source position is distinctly offset from the positions of the FU Orionis stars RNO 1B/1C which previously had been identified as sources of the observed outflow and as identical with IRAS

00338+6312. Minchin et al. (1991d) and Kastner et al. (1992) demonstrated that only one of the three intensity peaks in the Juggler nebula (AFGL 2136) was a source (Figure 12). Using the polarization map, they identified a bipolar reflection nebula likely produced by a molecular outflow and successfully predicted the outflow orientation from that of the polarization disk (Kastner et al. 1994).

In other cases, where the presence of a molecular outflow was established prior to the polarization mapping (for example, HL Tau, IRc2), the polarization disks always lie perpendicular to the known orientations of the outflows. Similar work in identifying likely outflow sources in bipolar reflection nebulae has been carried out for SVS 2 and SVS 20 in Serpens (Huard et al. 1997b), WK 34 in AFGL 437 (Weintraub and Kastner 1996), NGC 2024 FIR 4 (Moore and Yamashita 1995), GSS 30 (Weintraub et al. 1993; Tamura et al. 1991), R Mon (Minchin et al. 1991a), AFGL 2591 (Minchin et al. 1991b), and OMC-1 (Minchin et al. 1991c). It is also generally true that in cases where only aperture polarimetry exists, the position angle of the polarization of the unresolved star plus nebula will indicate the orientation of an outflow.

Figure 12a
Figure 12b

C. Polarization of Line Emission

The reflection nebula in OMC-1 shows a centrosymmetric pattern centered approximately on the position of IRc2 (Minchin et al. 1991c). This reflection nebula has been detected in both continuum and in molecular line emission from shocked H_2 in the v=1-0 S(1) line. Hough et al. (1986) (see also Burton et al. 1991; Chrysostomou et al. 1994) discovered that the inner portion of the reflection nebula, when observed in the H_2 line, is dichroically polarized. This is due to the presence of an extended region of material emitting S(1) photons that lies behind a medium of aligned grains. For now, this region of Orion is the only region known to show polarized line emission. Such regions may prove valuable for determining structure (i.e., alignment of grains) and magnetic field strengths, especially if additional regions of polarized line emission are discovered.

D. Circular Polarization

The measurement of circular polarization (CP) in the near-infrared has been pushed forward in the last few years through improved instrumentation. The Chamaeleon infrared nebula (Gledhill et al. 1996) and

GSS 30 in rho Ophiuchus (Chrysostomou et al. 1997) show evidence for CP in the near-infrared at levels of 1-2% while CP levels in OMC-1 (Bailey et al. 1998) reach an astounding 17%; most YSOs, however, show CP levels below 0.1% (Bastien et al. 1989). Several mechanisms have been suggested for producing CP, all of which involve polarization by scattering; however, the discovery of large (> 1%) CP is quite significant and will provide a challenge to the models. These methods for producing CP include multiple scattering off absorptive grains, single scattering off large, (magnetically) aligned grains, scattering of unpolarized incident photons off nonspherical, (magnetically) aligned grains and scattering of linearly polarized incident photons off spherical grains.

IV. CONCLUSIONS

In the 1990s, polarization studies have moved into the mainstream as an observational tool for astrophysics. Specifically, polarization studies provide information about dust grains. Measurements of intrinsically unpolarized starlight that becomes polarized as the result of passage through a dark cloud informs us directly that layers of dust grains exist in the cloud and that these dust grains have been aligned, probably by a magnetic field inside the cloud, producing a dichroic that polarizes background starlight. These same dust grains produce thermal radiation which, because of the preferred orientation imparted by the magnetic field, is intrinsically polarized. Finally, in the vicinity of YSOs, where dust grains grow in the shielded environments of cloud cores and dense, circumstellar disks, randomly oriented and sized dust grains will scatter photons from YSOs. These scattered light nebulae provide information about the sizes and types of dust grains, about the locations of YSOs which are detectable only through reflected light from the nebulae, and about the orientations of circumstellar disks and thereby the position angles of molecular outflows, where such outflows exist.

Acknowledgements. The research of DAW on polarization work is supported by a NASA Origins of Solar Systems grant. RLA gratefully acknowledges support from the Miller Institute for Basic Research in Science.

Acknowledgements. The research of DAW on polarization work is supported by a NASA Origins of Solar Systems grant. AAG is grateful to

the NASA-ISO program and the NSF Young Investigator program for supporting this work. RLA gratefully acknowledges support from the Miller Institute for Basic Research in Science. We thank Héctor Arce for his assistance with the Taurus data used to prepare Figure 2.

V. REFERENCES

Adams, F. C., Lada, C. J. and Shu, F. H. 1987. Spectral evolution of young stellar objects. *Astrophys. J.* 312:788–806.

Aitken, D. K., Smith, C. H., Morre, T. J. T., Roche, P. F., Fujiyoshi, T., and Wright, C. M. 1997. Mid- and far-infrared polarimetric studies of the core of OMC-1: the inner field configuration. *Mon. Not. Roy. Astron. Soc.* 286:85–96.

Akeson, R. L., and Carlstrom, J. E. 1997. Magnetic field structure in protostellar envelopes. *Astrophys. J.* 491:254–266.

Arce, H. G., Goodman, A. A., Bastien, P., Manset, N. and Sumner, M. 1998. The Polarizing Power of the Interstellar Medium in Taurus *Astrophys. J.* 499:L93–L96.

Bailey, J., Chrysostomou, A., Hough, J. H., Gledhill, T. M., McCall, A., Clark, S., Ménard, F., and Tamura, M. 1998. Circular polarization in star-formation regions: implications for biomolecular homochirality. *Science* 281: 672–675.

Bastien, P. 1988. Polarization properties of T Tauri stars and other pre-main sequence objects. In *Polarized radiation of circumstellar origin* (Vatican Observatory/University of Arizona Press), pp. 541–582.

Bastien, P. 1996. Polarization of young stellar objects. In *Polarimetry of the Interstellar Medium*, eds. W. G. Roberge and D. C. B. Whittet (San Francisco: Astronomical Society of the Pacific), pp. 297–314.

Bastien, P. and Ménard, F. 1988. On the interpretation of polarization maps of young stellar objects. *Astrophys. J.* 326:334–338.

Bastien, P. and Ménard, F. 1990. Parameters of disks around young stellar objects from polarization observations. *Astrophys. J.* 364:232–241.

Bastien, P., Robert, C., and Nadeau, R. 1989. Circular polarization in T Tauri stars. II. New observations and evidence for multiple scattering. *Astrophys. J.* 339:1089–1092.

Burton, M. G., Minchin, N. R., Hough, J. H., Aspin, C., Axon, D. J., and Bailey, J. A. 1991. Molecular hydrogen polarization images of OMC-1. scattering. *Astrophys. J.* 375:611–617.

Chrysostomou, A., Hough, J. H., Burton, M. G., and Tamura, M. 1994. Twisting magnetic fields in the core region of OMC-1. *Mon. Not. Roy. Astron. Soc.* 268:325–334.

Chrysostomou, A., Hough, J. H., Burton, M. G., and Tamura, M. 1994. Twisting magnetic fields in the core region of OMC-1. *Mon. Not. Roy. Astron. Soc.* 228:325–334.

Chrysostomou, A., Ménard, F., Gledhill, T. M., Clark, S., Hough, J. H., McCall, A., and Tamura, M. 1997. Polarimetry of young stellar objects - II. Circular polarization of GSS 30. *Mon. Not. Roy. Astron. Soc.* 285:750–758.

Dotson, J. L., 1996. Polarization of the far-infrared emission from M17. *Astrophys. J.* 470:566–576.

Dowell, C. D. 1997. Far-infrared polarization by absorption in the molecular cloud Sagittarius B2. *Astrophys. J.* 487:237–247.

Fischer, O., Henning, Th., and Yorke, H. W., 1994. Simulation of polarization maps. I. Protostellar envelopes. *Astron. Astrophys.* 284:187–209.

Fischer, O., Henning, Th., and Yorke, H. W., 1996. Simulation of polarization maps. II. The circumstellar environment of pre-main sequence objects. *Astron. Astrophys.* 308:863–885.

Galli, D. and Shu, F. H. 1993. Collapse of Magnetized Molecular Cloud Cores. I. Semianalytical Solution. *Astrophys. J.* 417:220–242.

Gerakines, P. A., Whittet, D. C. B. and Lazarian, A. 1995. Grain Alignment in the Taurus Dark Cloud. *Ap. J. (Letters)* 455:171–175.

Gledhill, T., Chrysostomou, A., and Hough, J. H. 1996. Linear and circular imaging polarimetry of the Chamaeleon infrared nebula. *Mon. Not. Roy. Astron. Soc.* 282:1418–1436.

Glenn, J., Walker, C. K., and Young, E. T. 1998. Magnetic Fields in Star Formation Regions: 1.3 mm Continuum Polarimetry. *Bull. Amer. Astron. Soc.* 192:1017 (abstract).

Gonatas, D. P., Engargiola, G. A., Hildebrand, R. H., Platt, S. R., Wu, X. D., Davidson, J. A., Novak, G., Aitken, A. K. and Smith, C. 1990. The far-infrared polarization of the Orion Nebula. *Astrophys. J.* 357:132–137.

Goodman, A. A. 1995. The Future of Magnetic Field Mapping in the Interstellar Medium. In *Airborne Astronomy Symposium on the Galactic Ecosystem: From Gas to Stars to Dust.* ed. M.R. Haas,

J.A. Davidson, and E.F. Erickson (San Francisco: ASP), p. 45.

Goodman, A. A., Bastien, P., Myers, P. C., and Ménard, F. 1990. Optical polarization maps of star-forming regions in Perseus, Taurus and Ophiuchus. *Astrophys. J.* 359:363–377.

Goodman, A. A., Jones, T. J., Lada, E. A. and Myers, P. C. 1992. The Structure of Magnetic Fields in Dark Clouds: Infrared Polarimetry in B216-217. *Astrophys. J.* 399: 108–113.

Goodman, A. A., Jones, T. J., Lada, E. A. and Myers, P. C. 1995. Does Near-Infrared Polarimetry Reveal the Magnetic Field in Cold Dark Clouds? *Astrophys. J.* 448: 748–765.

Greaves, J. S., Holland, W. S., and Ward-Thompson, D. 1997. Submillimeter polarimetry of class 0 protostars: Constraints on magnetized outflow models. *Astrophys. J.* 480:255–261.

Greaves, J. S., Murray, A. G., and Holland, W. S. 1994 Investigating the magnetic field structure around star formation cores. *Astron. Astrophys.* 284:L19–L22.

Greaves, J. S., et al., in prep.

Grinin, V. P. 1994. In *The Nature and Evolutionary Status of Herbig Ae/Be Stars*, eds. P. S. The, M. R. Perez, and P. J. van den Heuvel (San Francisco: Astronomical Society of the Pacific), pp. 63–.

Heiles, C. 1996. The Local Direction and Curvature of the Galactic Magnetic Field Derived from Starlight Polarization. *Astrophys. J.* 462: 316–325.

Heiles, C., Goodman, A. A., McKee, C. F., and Zweibel, E. G. 1993. Magnetic fields in star-forming regions: Observations. In *Protostars and Planets III*, eds. E. Levy and J. Levine (Tucson: Univ. of Arizona Press), pp. 279–326.

Heyer, M. H., Vrba, F. J., Snell, R. L., Schloerb, F. P., Strom, S. E., Goldsmith, P. F. and Strom, K. M. 1987. The Magnetic Evolution of the Taurus Molecular Clouds. I. Large-Scale Properties. *Astrophys. J.*,321:855–876.

Hildebrand, R. H. 1996. Problems in far-infrared polarimetry. In *Polarimetry of the Interstellar Medium*, eds. W. G. Roberge and D. C. B. Whittet (San Francisco: Astronomical Society of the Pacific), pp. 254–268.

Holland, W. S., Greaves, J. S., Ward-Thompson, D. and Andre, P. 1996 The magnetic field structure around protostars: submillimetre polarimetry of VLA 1623 and S106-IR/FIR. *Astron. Astrophys.*

309:267–274.

Hough, J. H., Axon, D. J., Burton, M. G., Gatley, I., Sato, S. Bailey, J., McCaughrean, M. J., McLean, I. S., Nagata, M., Allen, D. Garden, R. P., Hasegawa, T., Hayashi, M., Kaifu, N., Morimoto, M., and Walther, D. 1986. Infrared polarization in OMC-1 - Discovery of a molecular hydrogen reflection nebula. *Mon. Not. Roy. Astron. Soc.* 222:629–644.

Huard, T. C. 1998. unpublished.

Huard, T. C., Weintraub, D. A., and Kastner, J. H. 1997a. Polarization Modelling of Protostellar Environments with Large Dust Grain Distributions. *Bull. Amer. Astron. Soc.* 190:4106 (abstract).

Huard, T. C., Weintraub, D. A., and Kastner, J. H. 1997b. Bipolar Outflow Sources in the Serpens Core: SVS 2 and SVS 20. *Mon. Not. Roy. Astron. Soc.* 290:598–606.

Jones, T. J., Klebe, D. and Dickey, J.M. 1992. Infrared Polarimetry and the Galactic Magnetic Field II: Improved Models. *Astrophys. J.*, 389:602-615.

Kastner, J. H., and Weintraub, D.A. 1996. Water Ice in the Disk Around the Protostar AFGL 2136 IRS 1. *Astrophys. J.* 466: L103–L106.

Kastner, J. H., Weintraub, D. A., and Aspin, C. A. 1992. *The Juggler*: A Three-lobed Near-IR Reflection Nebula Toward CRL 2136 = OH17.6+0.2. *Astrophys. J.* 389:357–368.

Kastner, J. H., Weintraub, D. A., Snell, R. L., Sandell, G., Aspin, C., Hughes, D., and Baas, F. 1994. The Massive Molecular Outflow from CRL 2136 IRS 1. *Astrophys. J.* 425:695–706.

Kim, S., Martin, P. G., and Hendry, P. D. 1994. The size distribution of interstellar dust particles as determined from extinction. *Astrophys. J.* 422:164–175.

Lazarian, A., Goodman, A. A., and Myers, P. C. 1997. On the efficiency of grain alignment in dark clouds. *Astrophys. J.* 490:273–280.

Leach, R. W., Clemens, D. P., Kane, B. D., and Barvainis, R. 1991. Polarimetric mapping of Orion using Millipol: Magnetic activity in BN/KL. *Astrophys. J.* 370:257–262.

Leinert, C. H., Haas, M., and Lenzen, R. 1991. LkHα 198 and V376 Cassiopeiae - Speckle interferometric and polarimetric observations of circumstellar dust. *Astron. Astrophys.* 246:180–194.

Lucas, P. W., and Roche, P. F. 1997. Butterfly star in Taurus: struc-

tures of young stellar objects. *Mon. Not. Roy. Astron. Soc.* 286:895-919.

Lucas, P. W., and Roche, P. F. 1998. Imaging Polarimetry of Class I Young Stellar Objects. *Mon. Not. Roy. Astron. Soc.* 299:699–722.

Mathewson, D. S. and Ford, V. L. 1970. Polarization Observations of 1800 Stars. *Memoirs RAS* 74:139.

Mathis, J. S., Rumpl, W., and Nordsieck, K. H., 1977. The size distribution of interstellar grains. *Astrophys. J.* 217:425–433.

Ménard, F. Ph. D. Thesis, Université de Montréal.

Minchin, N. R., Bonifacio, V. H. R., and Murray, A. G. 1996. Submillimetre polarimetric observations of S140 and GL2591: investigating the role of viewing angle on observed polarization position angles. *Astron. Astrophys.* 315:L5–L8.

Minchin, N. R., Hough, J. H., McCall, A., Aspin, C., Yamashita, T., and Burton, M. G. 1991a. Near-infrared imaging polarimetry of bipolar nebulae — III. R Mon/NGC 2261. *Mon. Not. Roy. Astron. Soc.* 249:707–715.

Minchin, N. R., Hough, J. H., McCall, A., Aspin, C., Hayashi, S. S., Yamashita, T., and Burton, M. G. 1991b. Near-infrared imaging polarimetry of bipolar nebulae — II. GL 2591. *Mon. Not. Roy. Astron. Soc.* 251:508–521.

Minchin, N. R., Hough, J. H., McCall, A., Burton, M. G. , McCaughrean, M. J., Aspin, C., Bailey, J. A., Axon, D. J., and Sato, S. 1991c. Near-infrared imaging polarimetry of bipolar nebulae — I. The BN-KL region of OMC-1. *Mon. Not. Roy. Astron. Soc.* 248:715–729.

Minchin, N. R., Hough, J. H., Burton, M. G., and Yamashita, T. 1991d. Near-infrared imaging polarimetry of bipolar nebulae — IV. GL 490, GL 2789 and GL 2136. *Mon. Not. Roy. Astron. Soc.* 251:522–528.

Minchin, N. R. and Murray, A. G. 1994. Submillimetre polarimetric mapping of DR21 and NGC 7358-IRS 11: tracing the circumstellar magnetic field. *Astron. Astrophys.* 286:579–587.

Minchin, N. R., Sandell, G., and Murray, A. G. 1995. Submillimetre polarimetric observations of NGC 1333 IRAS 4A and 4B: tracing the circumstellar magnetic field. *Astron. Astrophys.* 293:L61–L64.

Moore, T. J. T., and Yamashita, T. 1995. A Near-infrared Reflection Nebula Associated with NGC 2024 FIR 4. *Astrophys. J.* 440:722–

727.

Moneti, A., Pipher, J.L., Helfer, H.L., McMillan, R.S. and Perry, M.L. 1984. Magnetic Field Structure in the Taurus Dark Cloud. *Astrophys. J.* 282:508–515.

Myers, P. C. and Goodman, A. A. 1991. On the Dispersion in Direction of Interstellar Polarization. *Astrophys. J.* 373: 509–524.

Nadeau, R., and Bastien, P. 1986. Circular polarization in T Tauri stars. *Astrophys. J.* 307:L5–L8.

Novak, G., Dotson, J. L., Dowell, C. D., Goldsmith, P. F., Hildebrand, R. H., and Schleuning, D. A. 1997. Polarized far-infrared emission from the core and envelope of the Sagittarius B2 molecular cloud. *Astrophys. J.* 487:320–327.

Ostriker, E., Gammie, C., and Stone, J. 1998, submitted.

Pendleton, Y. J., Tielens, A. G. G. M., and Werner, M. W. 1990. Studies of dust grain properties in infrared reflection nebulae. *Astrophys. J.* 349:107–119.

Rao, R., Crutcher, R. M., Plambeck, R. L., and Wright, M. C. H. 1998. High resolution millimeter-wave mapping of linearly polarized dust emission: magnetic field structure in Orion. *Astrophys. J.* 502:L75–L78.

Schleuning, D. A. 1998. Far-infrared and submillimeter polarization of OMC-1: Evidence for magnetically regulated star formation. *Astrophys. J.* 493:811–825.

Schleuning, D. A., Dowell, C. D., and Platt, S. R. 1996. Array polarimetry of the Orion Nebula from the Caltech Submillimeter Observatory. In *Polarimetry of the Interstellar Medium* eds. W. G. Roberge and D. C. B. Whittet (San Francisco: Astronomical Society of the Pacific), pp.254–268.

Schulz, A., Lenzen, R., Schmidt, T. and Proetel, K. 1981. Polarization of Starlight in M17. *Astron. Astrophys.* 95:94–99.

Tamura, M., Gatley, I., Joyce, R. R., Ueno, M., Suto, H., and Sekiguchi, M. 1991. Infrared Polarization Images of Star-forming Regions. I. The Ubiquity of Bipolar Structure. *Astrophys. J.* 378:611–627.

Tamura, M., Hough J. H., and Hayashi, S. S. 1995. 1 millimeter polarimetry of young stellar objects: low-mass protostars and T Tauri stars. *Astrophys. J.* 448:346–355.

Tamura, M., Nagata, T., Sato, S. and Tanaka, M. 1987. Infrared Polarimetry of Dark Clouds–I. Magnetic Field Structure in Heiles

Cloud 2. *Mon. Not. Roy. Astron. Soc.* 224:413–423.

Tamura, M., Yamashita, T., Sato, S., Nagata, T., and Gatley, I. 1988. Infrared polarimetry of dark clouds - III. The relationship between the magnetic field and star formation in the NGC 1333 region. *Mon. Not. Roy. Astron. Soc.* 231:445–453.

Terebey, S., Shu, F. H. and Cassen, P. 1984. The collapse of the cores of slowly rotating isothermal clouds. *Astrophys. J.* 286:529–551.

Turnshek, D. A., Turnshek, D. E., and Craine, E. R. 1980. Spectroscopic an polarimetric observations of NGC 1333 and the surrounding dark cloud complex. *Astron. J.* 85:1638–1643.

Vallée, J. P. and Bastien, P. 1996. Extreme-infrared (800 μm) polarimetry of the M17-SW molecular cloud with the JCMT. *Astron. Astrophys.* 313:255-268.

Weintraub, D. A., and Kastner, J. H. 1993. The Exciting Young Stellar Object for the Molecular Outflow at the Core of L1287. *Astrophys. J.* 411:767–772.

Weintraub, D. A., and Kastner, J. H. 1996. The Deeply Embedded Source That Drives the Protostellar Outflow in AFGL 437: Evidence From Near-Infrared Polarimetric Imaging. *Astrophys. J.* 458:670–679.

Weintraub, D. A., Kastner, J. H., Griffith, L. L., and Campins, H. C. 1993. Near-Infrared, Polarimetric Imaging of the Bipolar Lobes of GSS 30: Protostellar Infall or Outflow? *Astron. J.* 105:271–283.

Whitney, B., Kenyon, S. J., and Gomez, M. 1997. Near-Infrared Imaging Polarimetry of Embedded Young Stars in the Taurus-Auriga Molecular Cloud. *Astrophys. J.* 485:703–734.

Weintraub, D. A., Sandell, G., Huard, T. L., Kastner, J. H., van den Ancker, M. E., and Waters, R. 1999. Submillimeter Imaging of T Tauri's Circumbinary Disk and the Discovery of a Protostar in Hind's Nebula *Astrophys. J.*, in press.

Whitney, B., and Hartmann, L. 1993. Model scattering envelopes of young stellar objects. II - infalling envelopes. *Astrophys. J.* 402:605–622.

Whitney, B., and Hartmann, L. 1992. Model scattering envelopes of young stellar objects. II - Method and application to circumstellar disks. *Astrophys. J.* 395:529–539.

Whittet, D. C. B. 1992. Dust in the Galactic Environment. (Bristol: IOP Publishing)

Wilking, B. A., Lebofsky, M. J., Kemp, J. C., and Rieke, G. H. 1979. Infrared Polarimetry in the Rho Ophiuchus Dark Cloud. *Astron. J.* 84:199–203.

Wood, K., Kenyon, S. J., Whitney, B., and Turnbull, M. 1998. Optical and Near-infrared Model Images of the Circumstellar Environments of Classical T Tauri Stars. *Astrophys. J.* 497:404–418.

FIGURE CAPTIONS

Figure 1. Polarized light is produced by interstellar dust grains in three different ways: dichroic absorption by aligned dust grains, thermal radiation by aligned dust grains, and scattering of light by dust grains. The first two mechanisms rely on the systematic alignment of dust grains, usually by a magnetic field. In most magnetic alignment scenarios, the grain's short axis prefers to be parallel to the field (see Lazarian, Goodman, and Myers 1997.) Usually, scattered light is polarized, in the plane of the sky, along the direction perpendicular to the ray from the illuminating source to the scatterer.

Figure 2. Optical polarization map of Taurus superimposed on an ISSA 100 μm map. The horizontal white rectangle shows the location of the B216-217 dark cloud complex studied by Heyer et al. 1987 and Goodman et al. 1992 (see Figure 3, below). The vertical white rectangle shows the "cut" through Taurus studied by Arce et al. 1998 (see Figure 5, below). The polarization vectors shown are taken from (Moneti et al. 1984; Heyer et al. 1987; Goodman et al. 1990; and Arce et al. 1998). Figure courtesy of Héctor Arce.

Figure 3. Distribution of polarization position angle in the dark cloud B216-217. Fits of the Myers and Goodman 1991 model for polarization dispersion give statistically indistinguishable results for the optical data (Heyer et al. 1987) and the near-infrared data (Goodman et al. 1992). Figure reproduced from Goodman et al. 1992.

Figure 4. Observed relationships between polarization and extinction in dark clouds. *Top panel:* Data for filamentary dark clouds, L1755 and B216-217. *Lower panel:* Data for L1688, HCl 2, and NGC 1333, dark clouds which are closer to round, in projection, than L1755 and B216-217, and produce higher extinction. The box in the lower panel shows how small the range of polarization-extinction space covered by the "filamentary" clouds in the top panel is in comparison with the range for "round" clouds. Both panels show polarization near 2.2 microns on the y-axis. Dashed lines in each panel show error-weighted least-squares linear fits to the data points. Solid lines show the predictions of the Jones, Klebe and Dickey 1992 model, assuming equal non-uniform and uniform magnetic field energy. Figure based on Goodman et al. 1995.

Figure 5. Observed relation between polarization and extinction, where $A_V = 3.1 E_{B-V}$. The lines are least square linear fits, weighted by the uncertainty in p. The dashed line is the fit to points representing the stars background to the low-density ISM, which gives $p = (0.09 \pm 0.06) + (3.58 \pm 0.13) E_{B-V}$, with a correlation coefficient of 0.68. The solid line is the fit to the points representing the stars background to dark clouds, which gives $p = (1.61 \pm 0.13) + (0.03 \pm 0.15) E_{B-V}$, with a correlation coefficient of 0.79 (Figure reproduced from Arce et al. 1998).

Figure 6. W3 IRS 4 and 5: a) Grey scale image of total flux at 850 μm. b) Magnetic field vectors overlayed on contours of total flux at 850 μm - vector length is proportional to percentage polarization and direction

traces *B*. The field shows large-scale structure connecting the two cores, and polarization minima at the star-forming sites suggest field tangling. At a distance of 2.3 kpc, the largely uniform field covers ~1.4 pc. This map was obtained from 2 hours of integration with the SCUBA Polarimeter at the JCMT. (Figure courtesy of Antonio Chrysostomou and Jane Greaves).

Figure 7. *Left panel:* 100 micron polarization as observed with the KAO (Schleuning 1998). The bar at the top shows total polarized intensity. *Right panel:* 3 mm polarization as observed with the BIMA interferometer (Rao et al. 1998). The intensity peak of both maps is located near the position of IRc2. Note that at high spatial resolution, the apparent polarization hole near IRc2 shows significant non-uniform structure in the orientation of polarization vectors.

Figure 8. NGC 1333 IRAS 4A. a) The linearly polarized emission (grey scale) plotted with the total intensity (contours) for NGC 1333/IRAS 4A from Akeson and Carlstrom 1997. The contour levels are 25 mJy beam^{-1}. The FWHM of the beam (3.7″ by 2.8″ at a position angle of 74°) is shown in the lower left. b) The linearly polarized emission (grey scale) and two vectors of the polarization angle representing the range of angles seen in the data. The vectors shown are at angles of 97° and 109° (from Akeson and Carlstrom 1997).

Figure 9. A simulated reflection nebula with a source located at (0,0) and a disk aligned horizontally at y = 0. Most of the light from the central source singly scatters out of the nebula producing the centrosymmetric pattern. Some of the light multiply scatters into and out of the central disk plane, producing a linear region of low amplitude vectors along y = 0; this region is referred to as the "polarization disk." The small vectors along the disk plane are the result of the convolution of the true polarization signature of the nebula with the point spread function of the telescope (courtesy of Philip Lucas).

Figure 10. a) A comparison of Mie calculations for the scattering properties of small (MRN) and large (KHM) grains at 2.2 μm. The large grains are much more efficient at forward scattering these long wavelength photons. The small grains are better at back scattering (scattering angle > 90°), but their scattering efficiency is low at all angles at 2.2 μm. b) The MRN grains produce more highly polarized photons than the KMH grains at almost all scattering angles (from Huard 1998).

Figure 11. Simulated reflection nebulae at 2.2 μm, using a) small (MRN) and b) large (KMH) grain models. Each model follows 10^7 photons as they scatter through a disk of 100 AU, seen edge-on, and an envelope of 10,000 AU radii. Contours for the scattered intensity are at the 10 and 100 photon levels. Note how the model with KMH grains shows a much brighter nebula with far more photons back scattered toward the disk plane. This occurs because the KMH grains scatter so many more photons, even though the MRN grains are intrinsically better at back scattering (from Huard 1998).

Figure 12. a) Reflection nebula surrounding AFGL 2136 IRS 1. The base level contour is at 0.2 mJy arcsec^{-2} and the contour step is 0.3 mJy arcsec^{-2}. Offsets are in arcsec from AFGL 2136 IRS 1. Note that two of the three bright intensity peaks are pure scattered light; these peaks mark limb brightened walls of a an outflow cone oriented at position angle 135°. Note the "polarization disk" at position angle 45° (from Minchin

et al. 1991d). b) schematic of AFGL 2136 (from Kastner and Weintraub 1996).

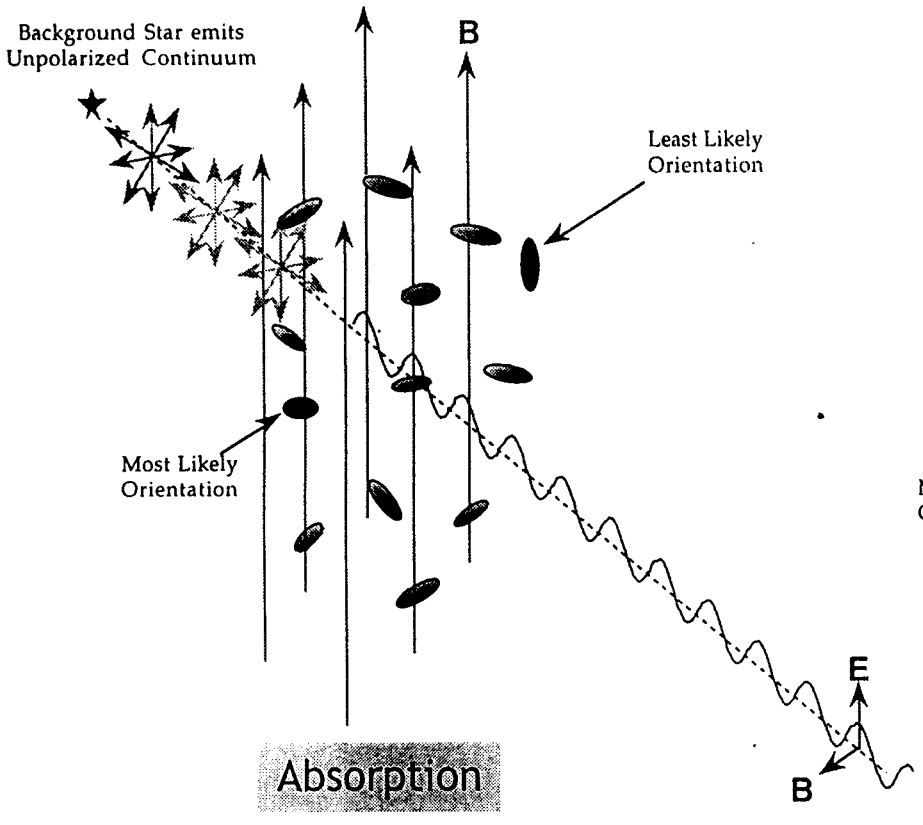

Absorption

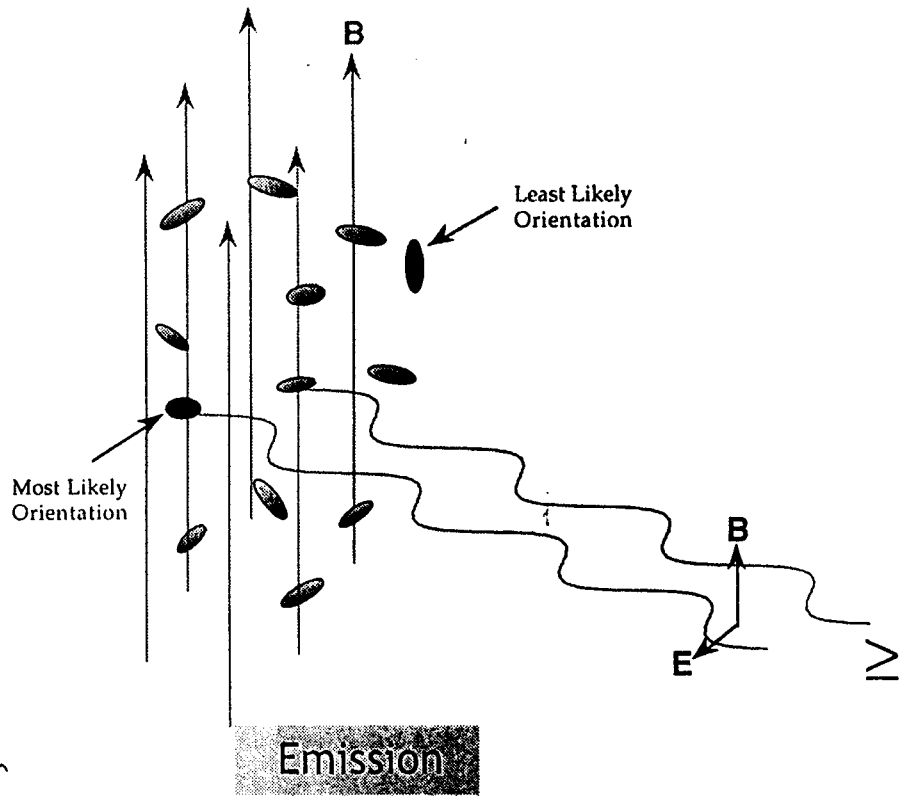

Emission

Scattering

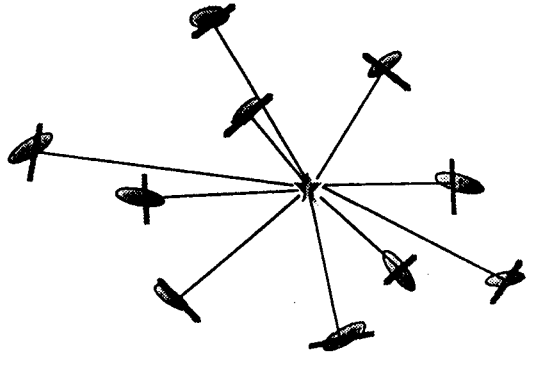

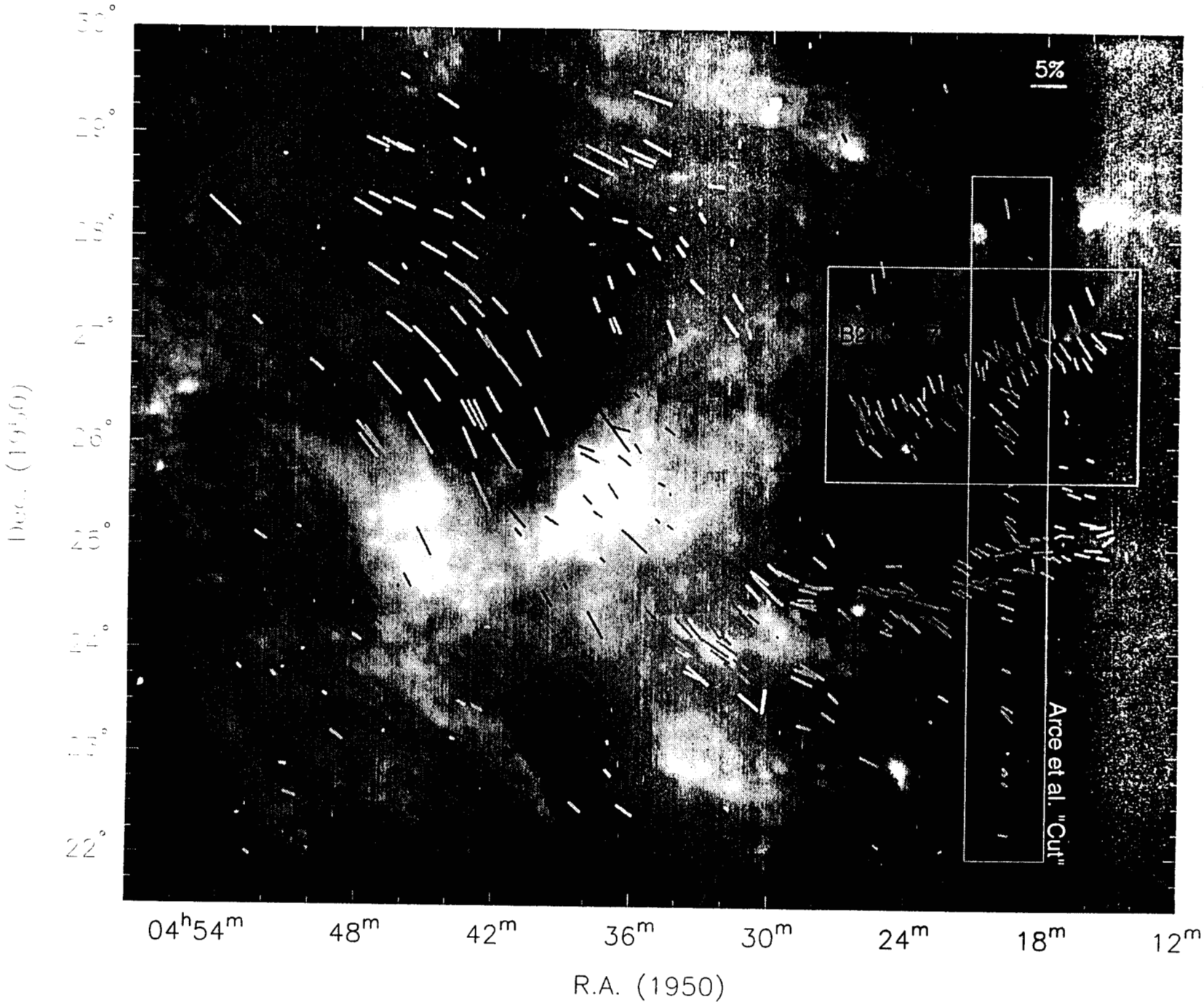
5%
B2
Arce et al. "Cut"
Dec. (1950)
22°
04h54m
48m
42m
36m
30m
24m
18m
12m
R.A. (1950)

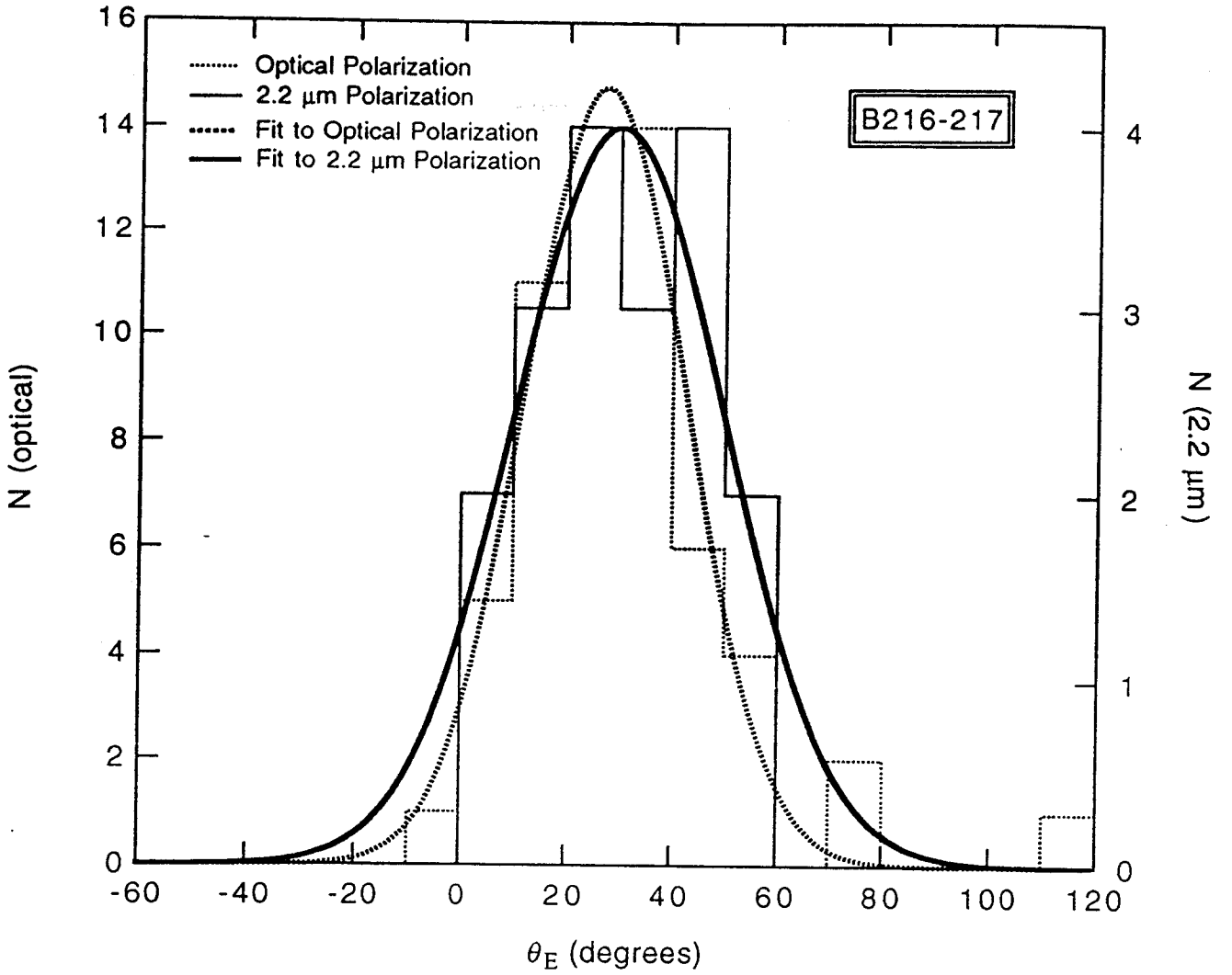
Optical Polarization
2.2 μm Polarization
Fit to Optical Polarization
Fit to 2.2 μm Polarization
B216-217
N (optical)
N (2.2 μm)
θE (degrees)
16
14
12
10
8
6
4
2
0
4
3
2
1
0
-60
-40
-20
0
20
40
60
80
100
120

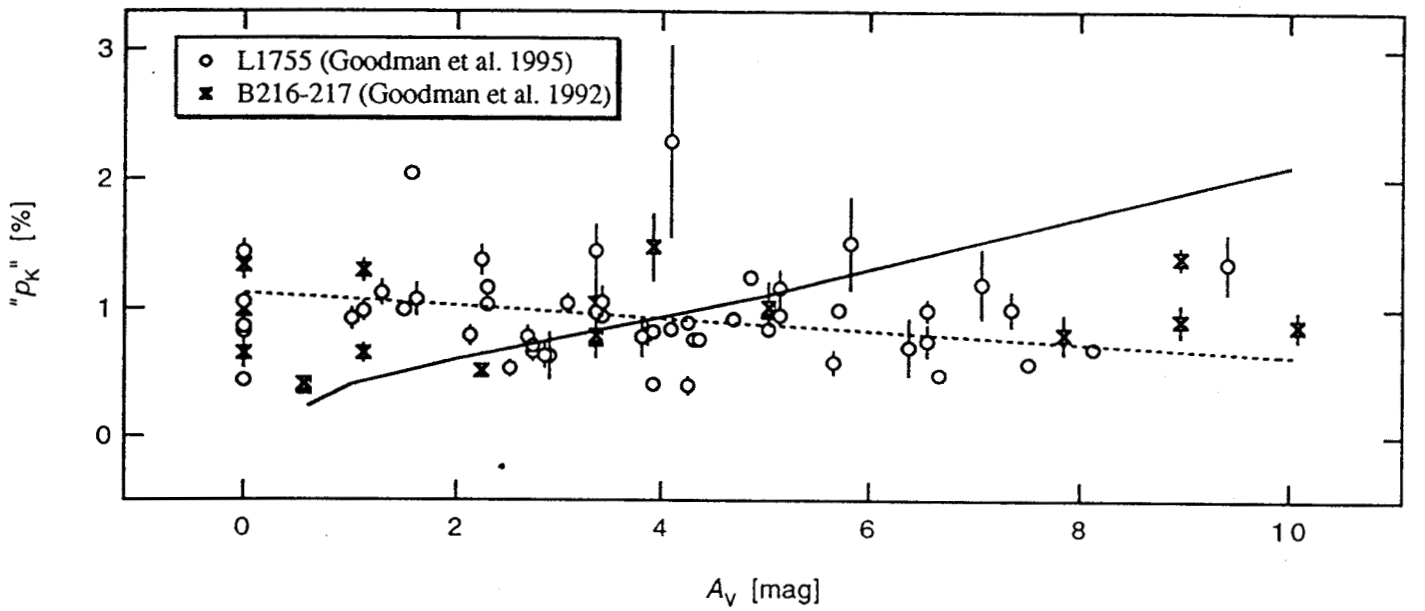
L1755 (Goodman et al. 1995)
B216-217 (Goodman et al. 1992)
"p_K" [%]
A_V [mag]

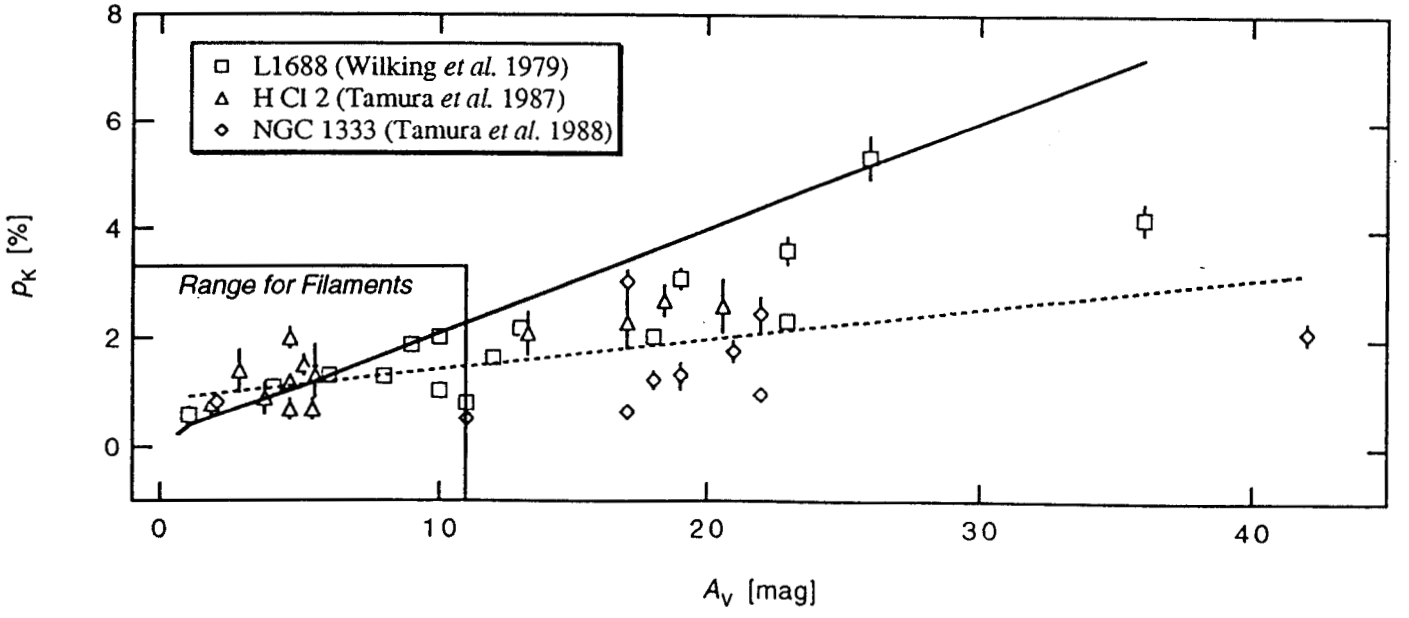
L1688 (Wilking *et al.* 1979)
H CI 2 (Tamura *et al.* 1987)
NGC 1333 (Tamura *et al.* 1988)
Range for Filaments
p_K [%]
A_V [mag]

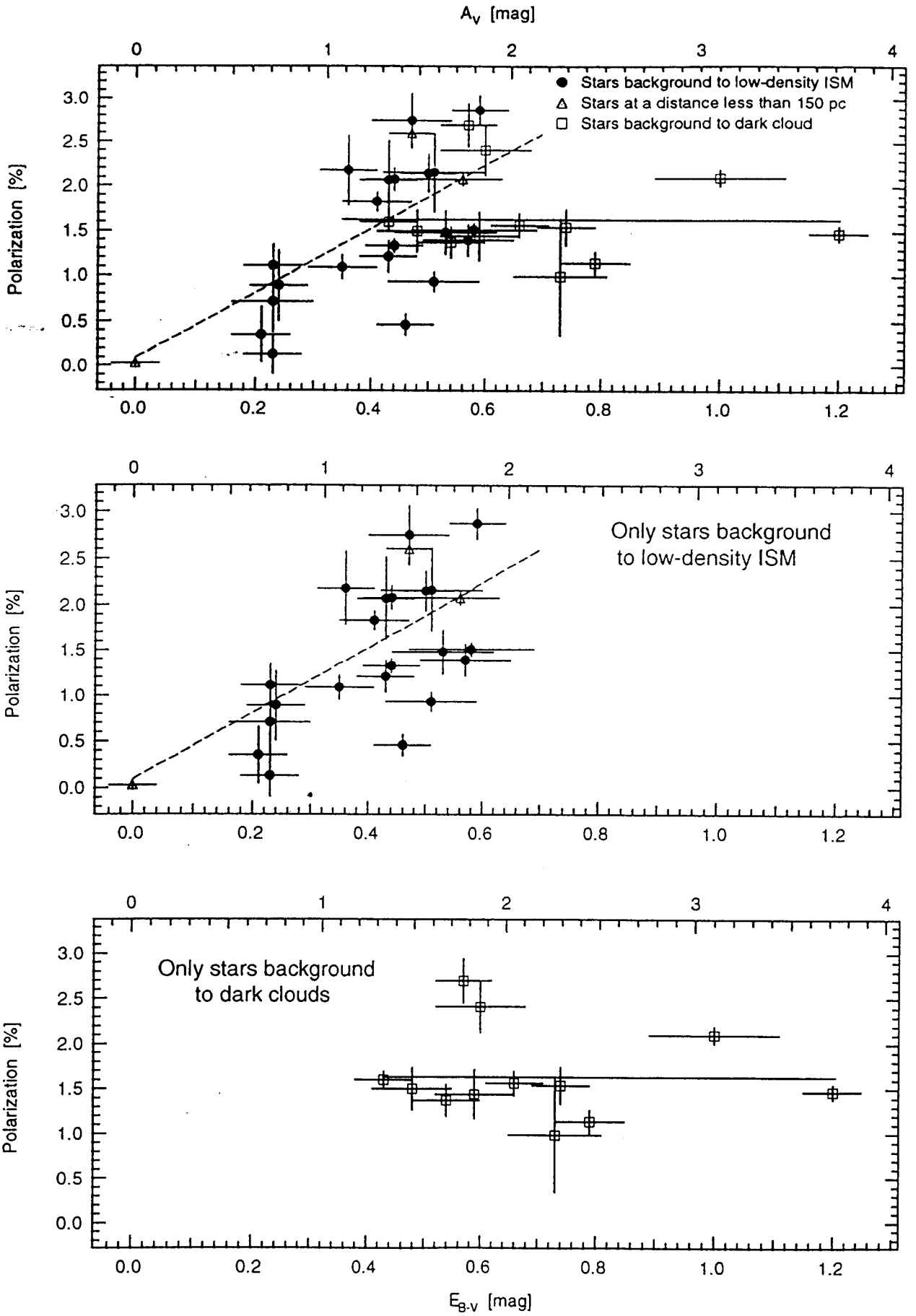
A_V [mag]
Stars background to low-density ISM
Stars at a distance less than 150 pc
Stars background to dark cloud
Polarization [%]
Only stars background to low-density ISM
Only stars background to dark clouds
E_{B-V} [mag]

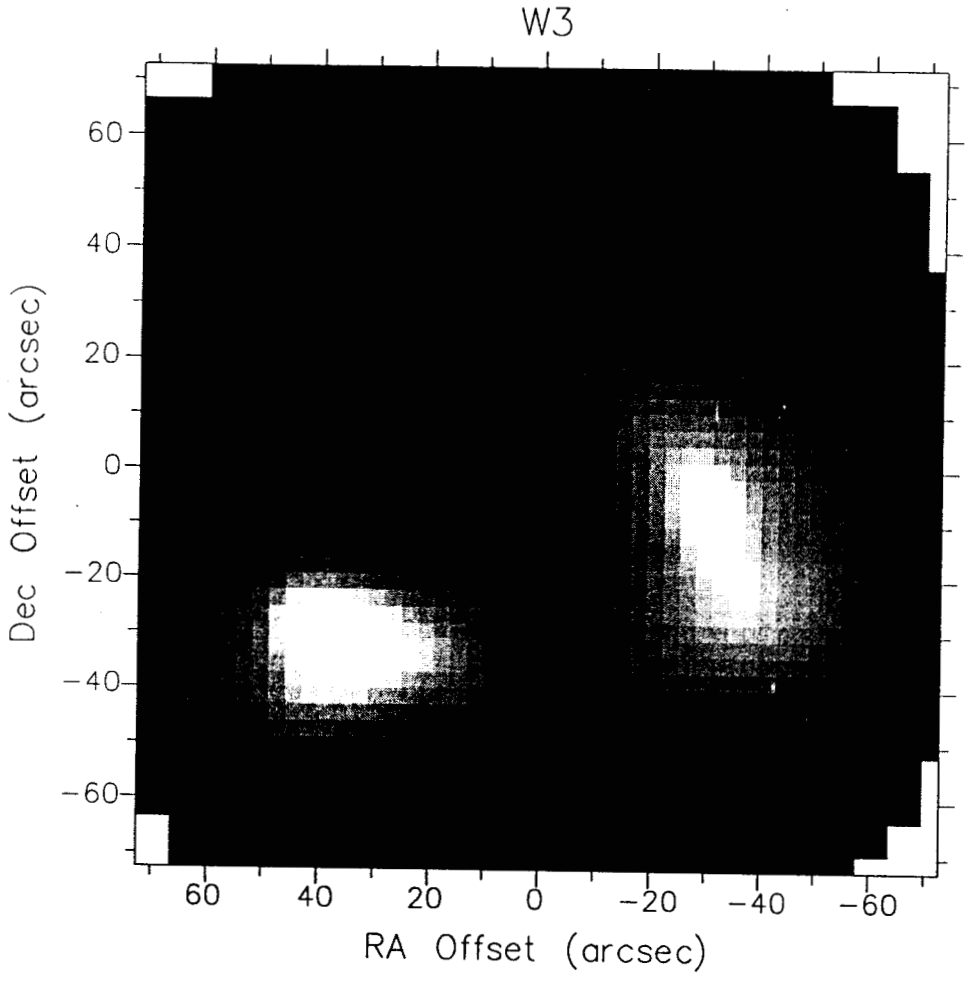
W3
60
40
20
0
−20
−40
−60
Dec Offset (arcsec)
60 40 20 0 −20 −40 −60
RA Offset (arcsec)

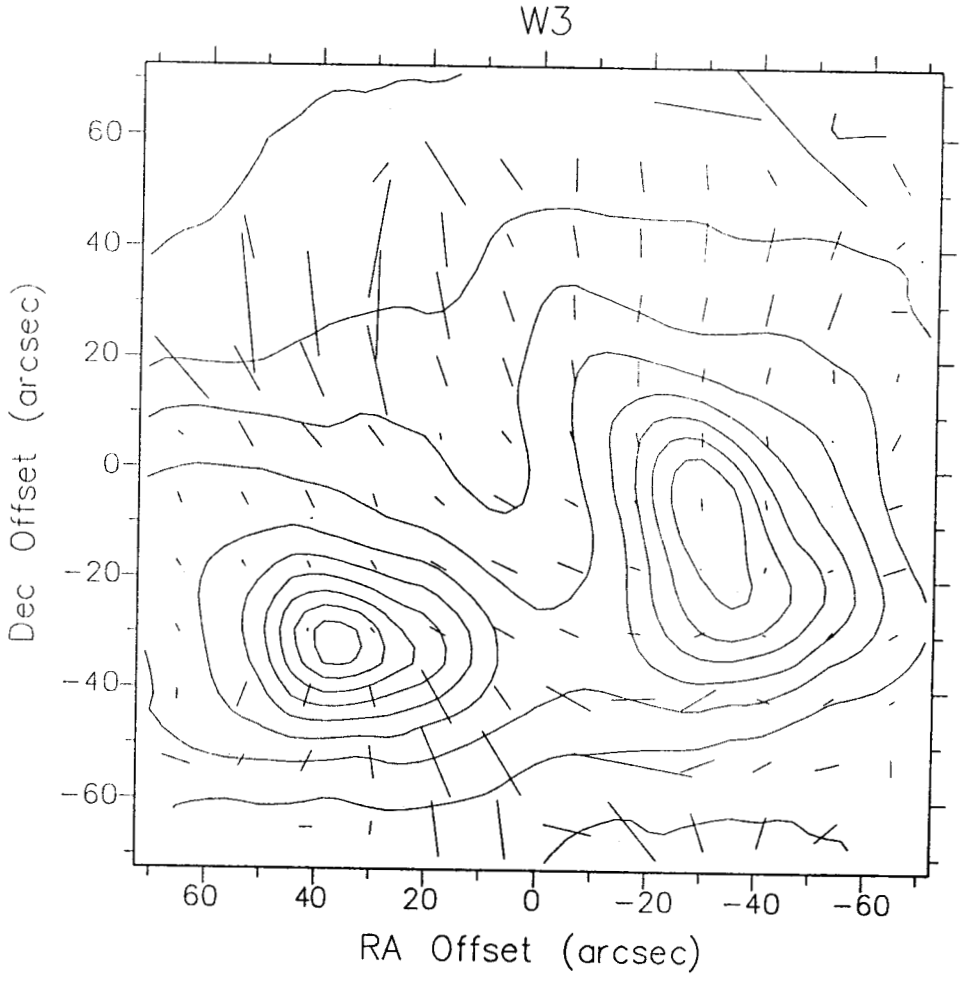
W3
60
40
20
0
−20
−40
−60
Dec Offset (arcsec)
60 40 20 0 −20 −40 −60
RA Offset (arcsec)

#7

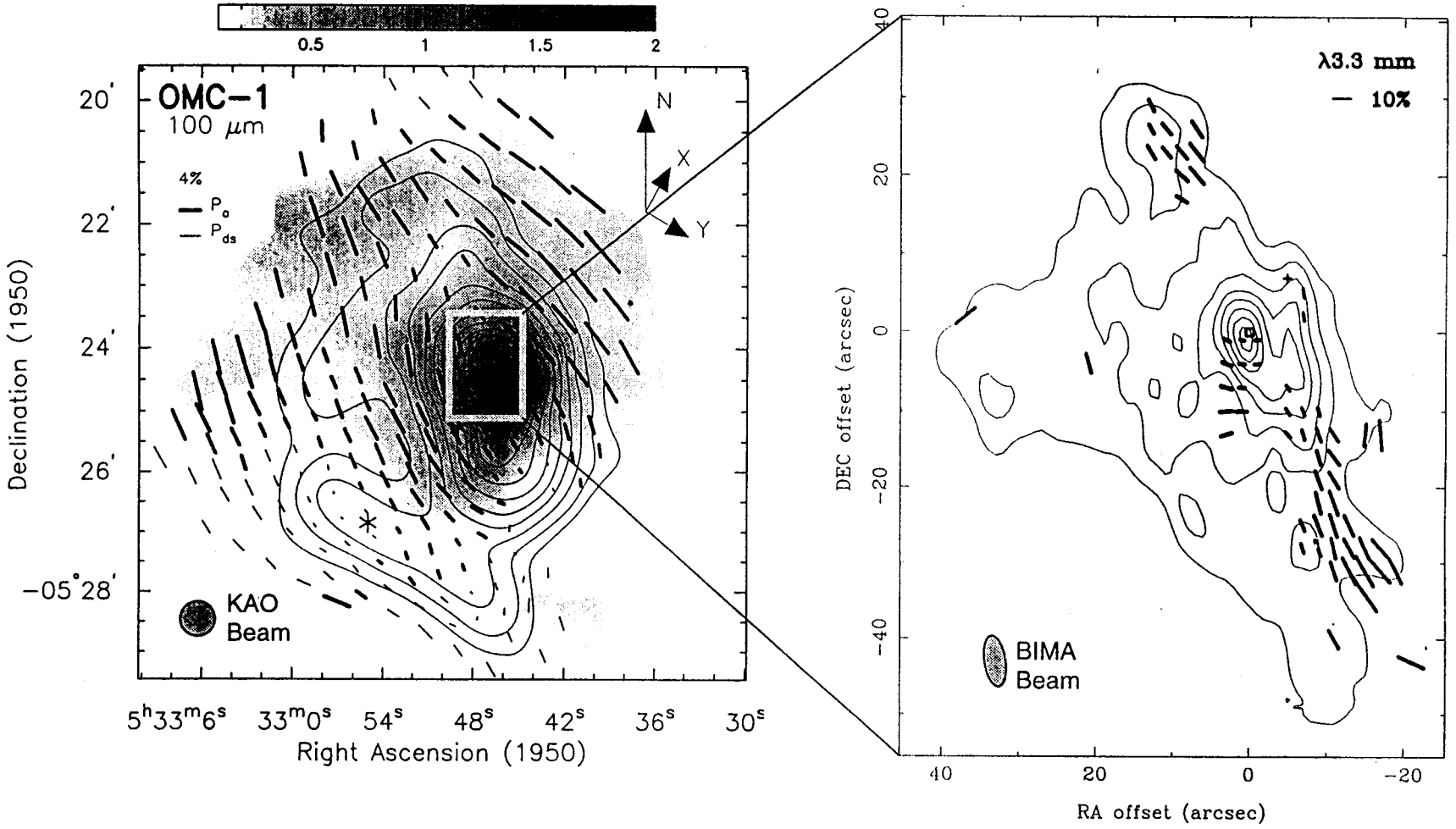
0.5
1
1.5
2
OMC–1
100 μm
4%
P_o
P_ds
N
X
Y
KAO
Beam
20'
22'
24'
26'
−05°28'
Declination (1950)
5h33m6s
33m0s
54s
48s
42s
36s
30s
Right Ascension (1950)
λ3.3 mm
— 10%
BIMA
Beam
DEC offset (arcsec)
RA offset (arcsec)
40
20
0
−20
−40

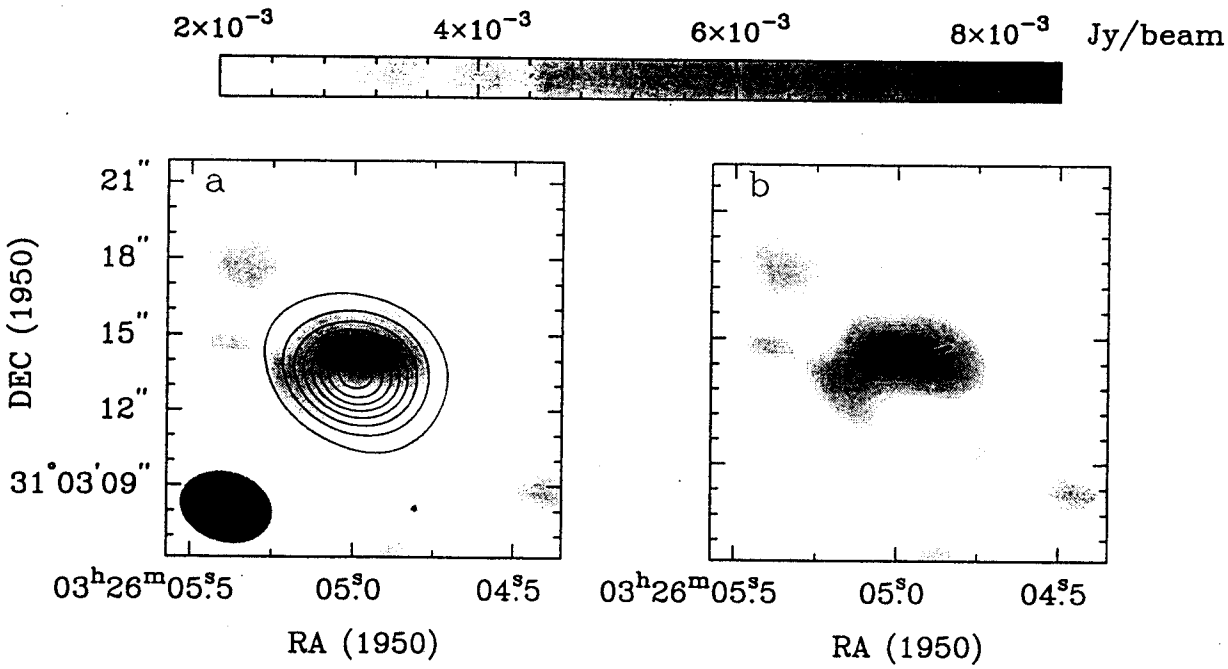
2×10⁻³
4×10⁻³
6×10⁻³
8×10⁻³
Jy/beam
a
b
21″
18″
15″
12″
31°03′09″
DEC (1950)
03h26m05s5
05s0
04s5
RA (1950)
03h26m05s5
05s0
04s5
RA (1950)

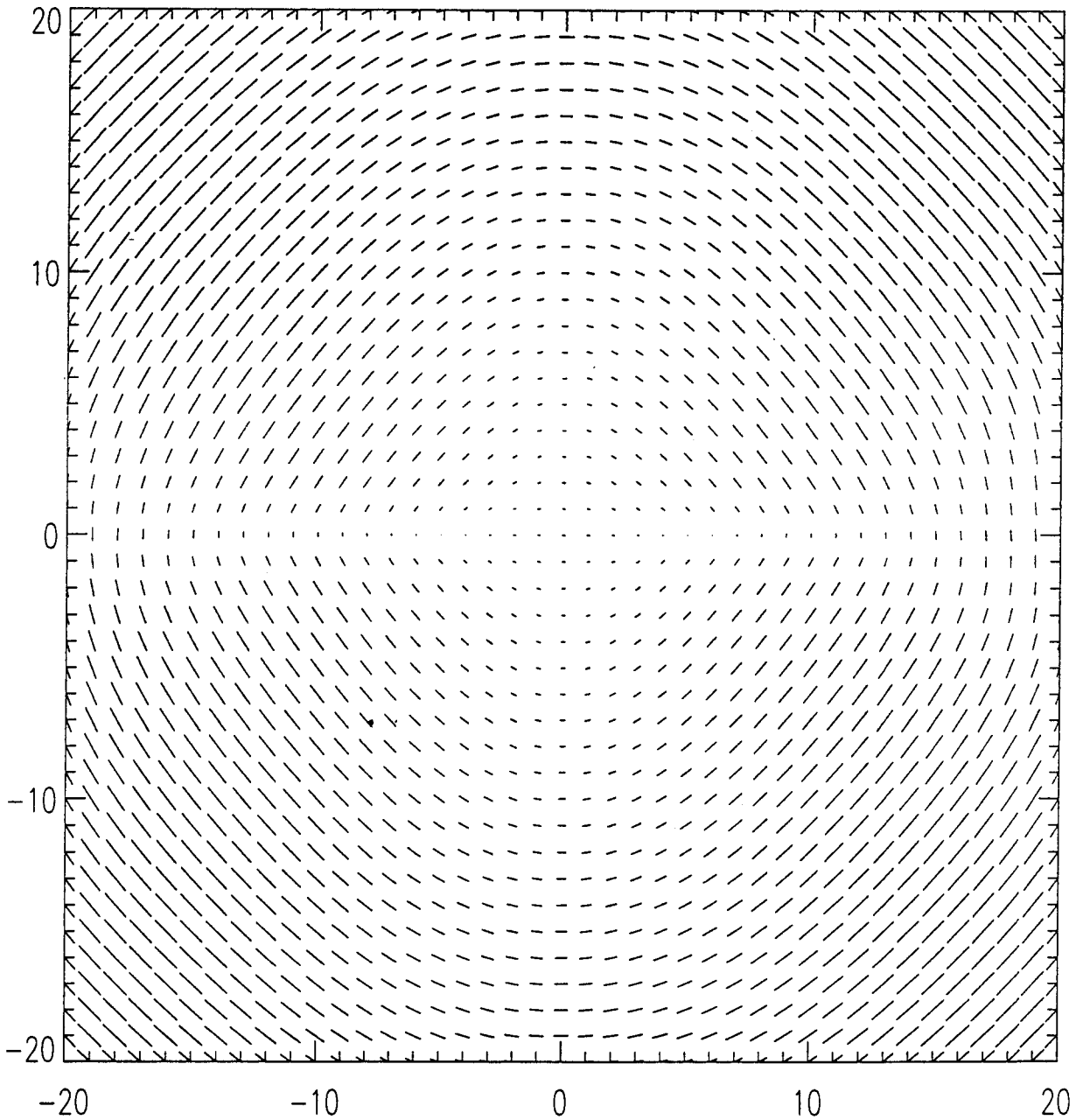
20
10
0
−10
−20
−20
−10
0
10
20

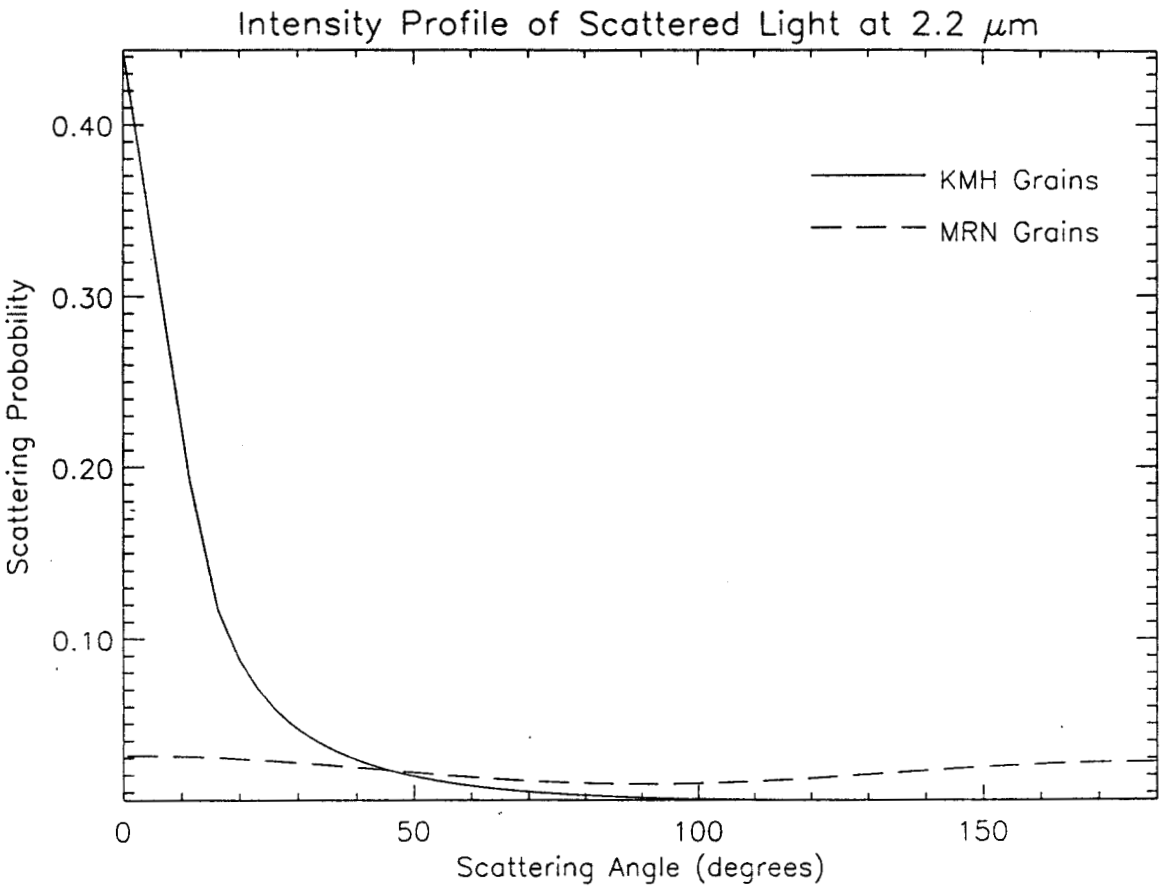
Intensity Profile of Scattered Light at 2.2 μm
Scattering Probability
0.40
0.30
0.20
0.10
KMH Grains
MRN Grains
0
50
100
150
Scattering Angle (degrees)

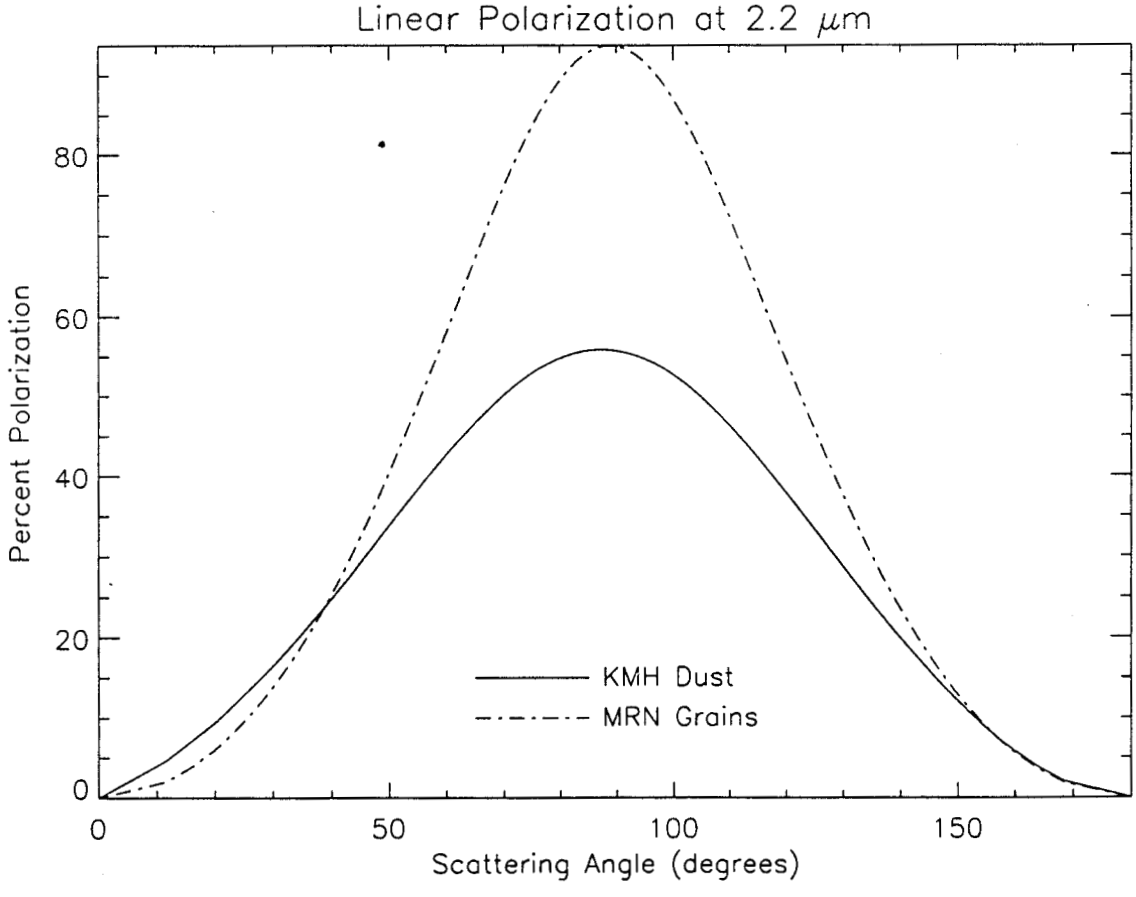
Linear Polarization at 2.2 μm
Percent Polarization
80
60
40
20
0
KMH Dust
MRN Grains
0
50
100
150
Scattering Angle (degrees)

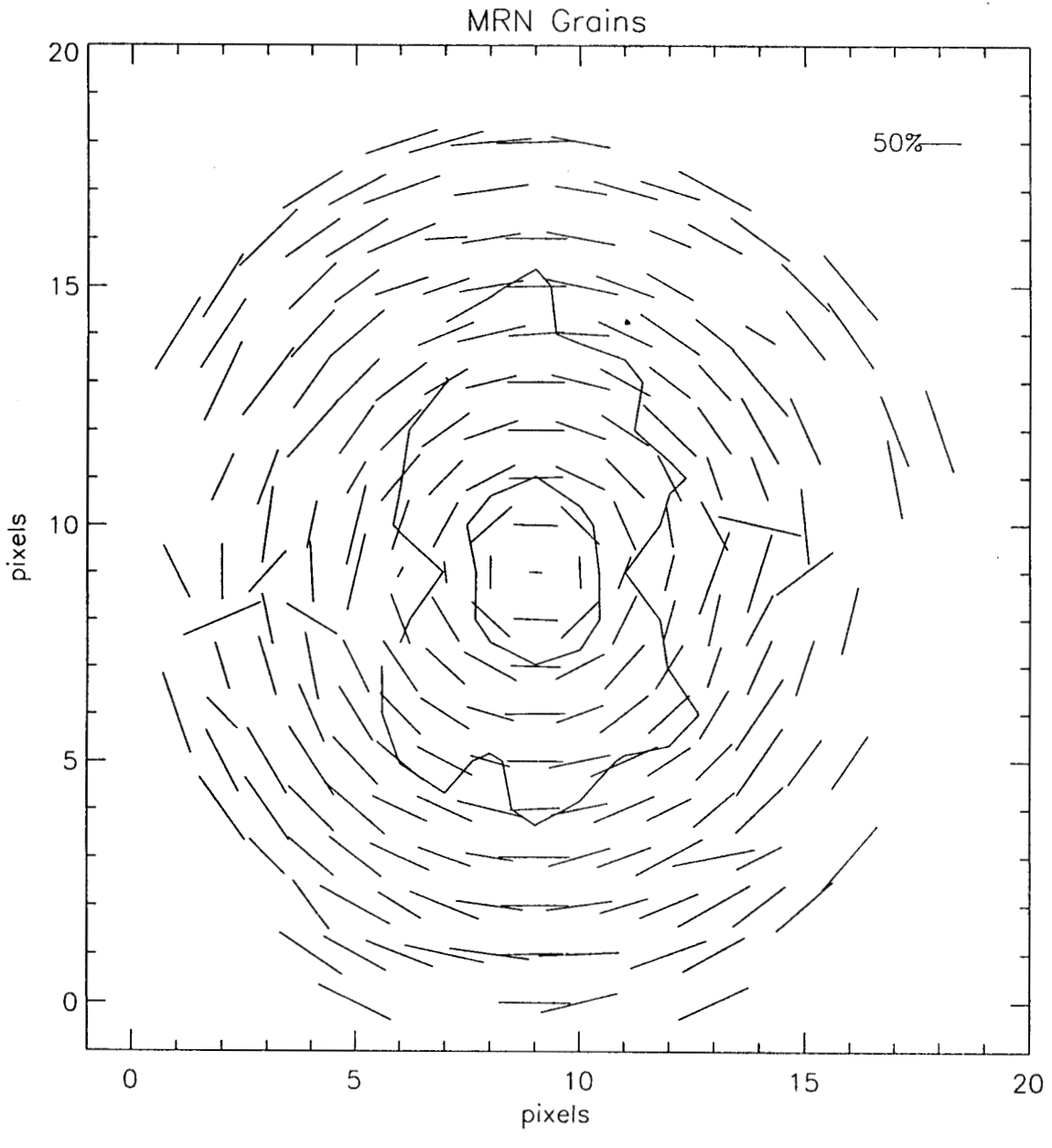
MRN Grains
50%
pixels
pixels
0
5
10
15
20

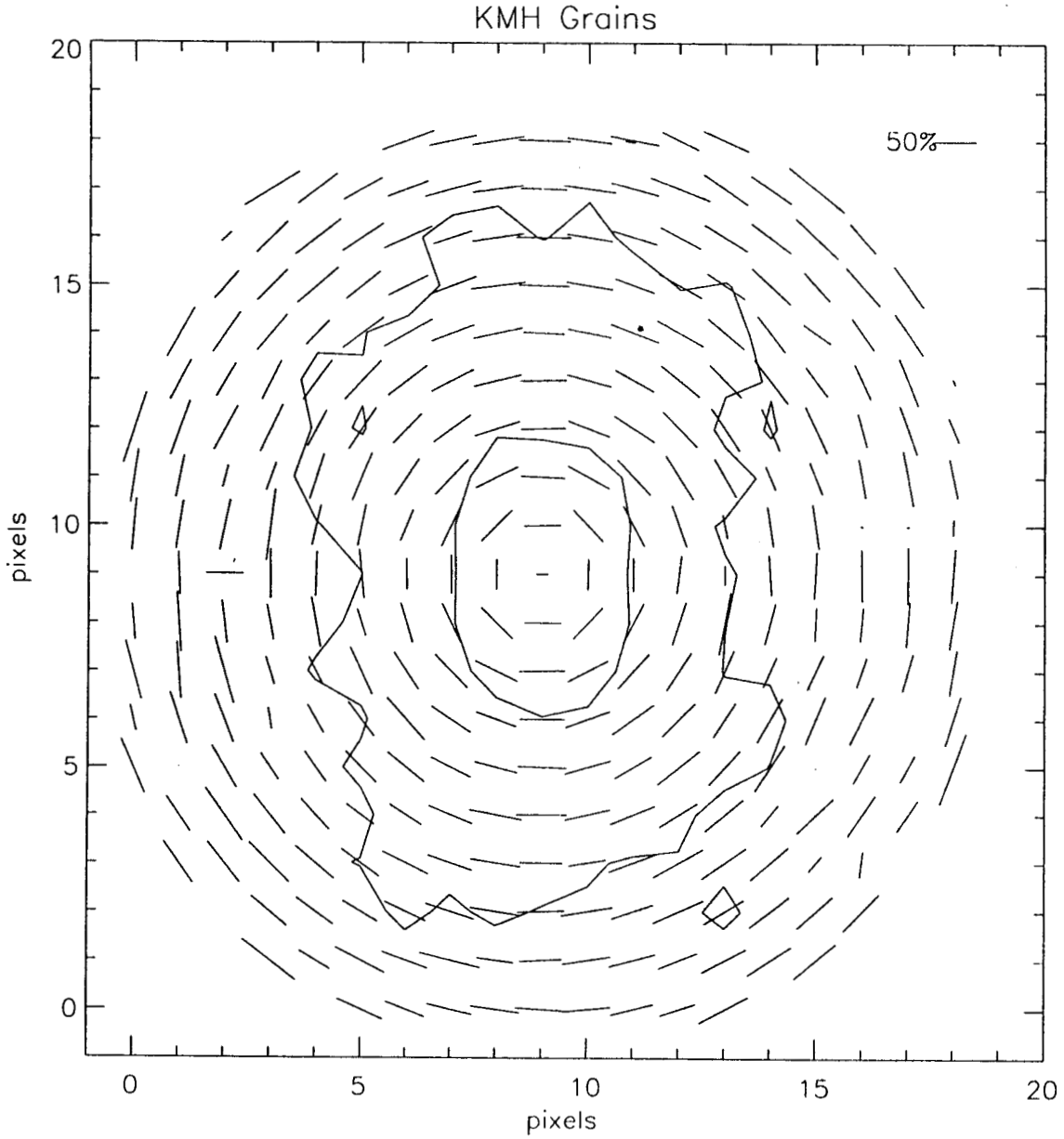
KMH Grains
50%
pixels
pixels
0
5
10
15
20

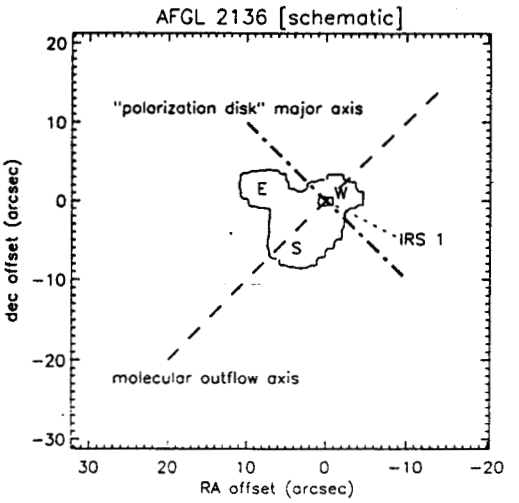
AFGL 2136 [schematic]
"polarization disk" major axis
E
W
S
IRS 1
molecular outflow axis
dec offset (arcsec)
RA offset (arcsec)
20
10
0
−10
−20
−30
30
20
10
0
−10
−20

#12a